Available online at www.sciencedirect.com
ScienceDirect
Geochimica et Cosmochimica Acta 74 (2010) 2741–2759
Geochimica et Cosmochimica Acta
www.elsevier.com/locate/gca

High-precision high field strength element partitioning between garnet, amphibole and alkaline melt from Kakanui, New Zealand

Eric C. Fulmer [a,*], Oliver Nebel [a,b], Wim van Westrenen [a]

[a] Faculty of Earth and Life Sciences, VU University Amsterdam, De Boelelaan 1085, 1081 HV Amsterdam, The Netherlands
[b] Research School of Earth Sciences, The Australian National University, Mills Road, 0200 ACT Canberra, Australia

Received 24 September 2009; accepted in revised form 12 February 2010; available online 23 February 2010

Abstract

The high field strength elements (HFSE: Zr, Hf, Nb, Ta, and W) are an important group of chemical tracers that are increasingly used to investigate magmatic differentiation processes. Successful modeling of these processes requires the availability of accurate mineral–melt partition coefficients (D). To date, these have largely been determined by ion microprobe or laser ablation-ICP-MS analyses of the run products of high-pressure, high-temperature experiments. Since HFSE are (highly) incompatible, relatively immobile, high-charge, and difficult to ionize, these experiments and their analysis are challenging. Here we explore whether high-precision analyses of natural mineral–melt systems can provide additional constraints on HFSE partitioning.

The HFSE concentrations in natural garnet and amphibole and their alkaline host melt from Kakanui, New Zealand are determined with high precision isotope dilution on a multi-collector-ICP-MS. Major and trace element compositions combined with Lu–Hf isotopic systematics and detailed petrographic sample analysis are used to assess mineral–melt equilibrium and to provide context for the HFSE D measurements. The whole-rock nephelinite, ~1 mm sized amphiboles in the nephelinite, and garnet megacrysts have similar initial Hf isotope ratios with a mean initial $^{176}Hf/^{177}Hf_{(34\ Ma)} = 0.282900 \pm 0.000026$ (2σ). In contrast, the amphibole megacrysts are isotopically distinct ($^{176}Hf/^{177}Hf_{(34\ Ma)} = 0.282830 \pm 0.000011$). Rare earth element D values for garnet megacryst–nephelinite melt and ~1 mm amphibole–nephelinite melt plotted as a function of ionic radii show classic near-parabolic trends that are in excellent agreement with crystal lattice-strain models. These observations are consistent with equilibrium between the whole-rock nephelinite, the ~1 mm amphibole grains within the nephelinite and the garnet megacrysts.

High-precision isotope dilution results for Zr and Hf in garnet ($D_{Zr} = 0.220 \pm 0.007$ and $D_{Hf} = 0.216 \pm 0.005$ [2σ]), and for all HFSE in amphibole are consistent with previous experimental findings. However, our measurements for Nb and Ta in garnet ($D_{Nb} = 0.0007 \pm 0.0001$ and $D_{Ta} = 0.0011 \pm 0.0006$ [2σ]) show that conventional methods may overestimate Nb and Ta concentrations, thereby overestimating both Nb and Ta absolute D values for garnet by up to 3 orders of magnitude and underestimating D_{Nb}/D_{Ta} by greater than a factor of 100. As a consequence, the role of residual garnet in imposing Nb/Ta fractionation may be less important than previously thought. Moreover, garnet $D_{Hf}/D_W = 17$ and $D_{Nb}/D_{Zr} = 0.003$ imply fractionation of Hf from W and Nb from Zr upon garnet crystallization, which may have influenced short-lived ^{182}Hf–^{182}W and ^{92}Nb–^{92}Zr isotopic systems in Hadean time.

1. INTRODUCTION

The high field strength elements (HFSE: Zr, Hf, Nb, Ta, and W) have become a key group of trace elements in

* Corresponding author.
E-mail address: ecfulmer@gmail.com (E.C. Fulmer).

0016-7037/$ - see front matter © 2010 Elsevier Ltd. All rights reserved.
doi:10.1016/j.gca.2010.02.020

igneous petrology. They are commonly used as sensitive tracers for magmatic processes in Earth's major silicate reservoirs and have been used to study the depleted mantle (Salters and Zindler, 1995; Blichert-Toft and Albarède, 1997; Chauvel and Blichert-Toft, 2001; Weyer et al., 2003; Chauvel et al., 2008), ocean island basalts (Patchett, 1983; Salters and Hart, 1991; David et al., 2000; Pfänder et al., 2007b), subduction zones (White and Patchett, 1984; Pearce et al., 1999; Woodhead et al., 2001; Münker et al., 2004; Tollstrup and Gill, 2005; Nebel et al., 2007a; König et al., 2008; Chauvel et al., 2009; Schmidt et al., 2009), and sediments and continental crust (Patchett et al., 1981; Vervoort and Patchett, 1996; Amelin et al., 1999; Barth et al., 2000; Bizzarro et al., 2003; Harrison et al., 2005; Nebel et al., 2007a,b, 2010), as well as large-scale planetary differentiation (Münker et al., 2003; Touboul et al., 2007). In addition, HFSE form part of the widely used long-lived ^{176}Lu–^{177}Hf and subordinately the short-lived ^{182}Hf–^{182}W and ^{92}Nb–^{92}Zr isotopic systems. Lutetium–Hf systematics have become a robust and powerful complement to the Sm–Nd system, providing insight into the long-term evolution of the depleted mantle and continental crust (e.g., Vervoort and Blichert-Toft, 1999; Vervoort et al., 2000, 2007). Significant interest in the Hf–W system has developed due to its ability to constrain early core–mantle differentiation (Kleine et al., 2002; Schoenberg et al., 2002a; Yin et al., 2002) and core–mantle interaction (Schoenberg et al., 2002b; Scherstén et al., 2004), whereas Nb–Zr is dominantly used for early solar system chronology (Harper, 1996; Münker et al., 2000; Schönbächler et al., 2002, 2003).

The HFSE include two isovalent element pairs Zr–Hf ($HFSE^{4+}$) and Nb–Ta ($HFSE^{5+}$) with nearly equal ionic radii that have very similar chemical properties. These pairs are expected to behave nearly identically in both fluids and melts in comparison to most other groups of trace elements with similar incompatibility (e.g., U–Th and Ce–Pb) and their ratios were long thought to be constant in the major reservoirs of the silicate Earth. However, a growing data set aided by significant analytical improvements (Blichert-Toft et al., 1997; Weyer et al., 2002) has revealed resolvable and significant differences in Zr/Hf and Nb/Ta in a wide range of terrestrial and extraterrestrial rocks (Barth et al., 2000; Münker et al., 2003; Weyer et al., 2003; Pfänder et al., 2007a,b).

The majority of terrestrial silicate rock samples plot roughly along a so called Zr/Hf–Nb/Ta silicate fractionation trend (Pfänder et al., 2007b). A notable feature for this global correlation is that all terrestrial rocks plot significantly below chondritic Nb/Ta values, while Zr/Hf ratios are observed to be both super- and sub-chondritic (Münker et al., 2003). The Nb/Ta ratios of the two major silicate reservoirs accessible to field studies (i.e., the upper mantle and the continental crust) are almost exclusively below the chondritic ratio ($Nb/Ta = 19.9 \pm 0.6$, Münker et al., 2003), leading to the interpretation that the silicate portion of the Earth is Nb-deficit. Several hypotheses have therefore been put forward to account for the "missing" Nb, including the presence of an isolated refractory reservoir of super-chondritic Nb/Ta subducted eclogite in the lower mantle (McDonough, 1991; Barth et al., 2000; Kamber and Collerson, 2000; Rudnick et al., 2000; Rapp et al., 2003; Pfänder et al., 2007b), or incorporation of Nb into the core during planetary differentiation (Wade and Wood, 2001).

In order to quantitatively model the evolution of HFSE concentrations and to predict fractionation between radiogenic parent and daughter elements during magmatic processes, well-constrained partition coefficients D between mineral phases and melts are required (where D is the concentration ratio between mineral and melt; Beattie, 1993). Early partitioning studies focused on analysis of naturally occurring phenocryst-melt pairs for a wide range of minerals and melt compositions (Philpotts and Schnetzler, 1970; Schnetzler and Philpotts, 1970; Irving and Frey, 1978, 1984). However, as trace element partitioning is strongly affected by pressure, temperature, and mineral/melt composition, efforts in the past 20+ years have shifted almost exclusively to experiments. Partition coefficients for HFSE are currently determined mostly using ion microprobe or laser ablation-ICP-MS analyses of the run products of high-pressure, high-temperature experiments (e.g., Brenan et al., 1994, 1995; Ionov and Hofmann, 1995; LaTourrette et al., 1995; van Westrenen et al., 1999; Foley et al., 2000; Tiepolo et al., 2000b, 2001; Klemme et al., 2002; Green and Adam, 2003; Righter and Shearer, 2003; Schmidt et al., 2004; Xiong et al., 2005; Klimm et al., 2008).

The HFSE are (highly) incompatible in most mantle phases, relatively immobile in fluids, and high-charge, causing HFSE partitioning experiments and their analysis to be challenging. For example, as the charge-balancing mechanisms for trace-level high-charge cations in natural silicates and oxides are poorly known, it is difficult to decide which, if any, charge-balancing cation(s) need(s) to be added to synthetic starting materials. As a result it is difficult to ascertain if data obtained from experiments using starting materials with elevated HFSE contents are applicable to natural rock systems that usually have much lower HFSE contents. In addition, the HFSE are difficult to ionize, complicating their analyses by e.g., ion microprobe. These inherent difficulties of studying HFSE partitioning in experimental systems, coupled with the dramatic improvements in HFSE natural rock analytical techniques, prompted us to explore whether high-precision analyses of natural mineral–host melt systems can provide improved constraints on HFSE partitioning.

High-precision HFSE concentrations of garnet and amphibole, two important trace element-bearing mantle minerals, and the nephelinitic host melt from the Kakanui Mineral Breccia (KMB), Kakanui, New Zealand (Dickey, 1968; Mason, 1968) were determined with isotope dilution on a MC-ICP-MS. Additional trace element concentrations were determined with a single-collector-ICP-MS to provide context. Garnet was chosen because it plays a critical role in trace element distribution in the mantle and has been widely studied for many years in experimental petrology. The role of garnet in HFSE fractionation in particular has also recently been debated (van Westrenen et al., 2001a; Pertermann et al., 2004; Klimm et al., 2008). Amphibole is a recognized major host of HFSE in the subcontinental lithospheric mantle (SCLM) and may play an important role in the generation of continental basalts, mantle metasomatism

and fractional crystallization in hydrous melts. Amphibole may also be able to significantly fractionate Nb and Ta from Zr and Hf (Tiepolo et al., 2000a,b, 2001).

The study of natural instead of experimental systems comes with its own difficulties, including the generally low trace element concentrations in mineral phases of interest and the possibility of open system behavior. While the isotope dilution technique provides a solution for the analytical difficulties of very low trace element concentrations, particular care must be taken to demonstrate chemical equilibrium between mineral and host melt for the trace elements in question. Here, we address this issue using a combined approach including detailed sample petrography, Lu–Hf isotope systematics, crystal lattice-strain partitioning theory, and Fe–Mg exchange thermometry.

2. SAMPLE DESCRIPTION AND PETROGRAPHY

The Kakanui Mineral Breccia (KMB) is a well-studied shallow-marine volcano-clastic deposit located near Kakanui, New Zealand, on the eastern coast of the South Island and is a member of the Deborah Volcanic Formation (Dickey, 1968; Mason, 1968; White et al., 1972; Mason and Allen, 1973; Merrill and Wyllie, 1975; Zack et al., 1997; Corcoran and Moore, 2008). The KMB is composed of a mela-nephelinite host melt that is notable for its abundant, up to fist-sized, medium-grained polycrystalline nodules of lherzolite, pyroxenite, hornblendite, and eclogite [hereafter referred to as amphibole-garnet-clinopyroxene (amph-grt-cpx) nodules], as well as granulite. Also present in the KMB are large single crystal fragments (hereafter megacrysts) of pyrope-rich garnet, kaersutitic amphibole, and Al-rich clinopyroxene. The mela-nephelinite host melt groundmass contains a very fine-grained mat of titaniferous augite laths, skeletal apatite prisms, titanomagnetite grains, and micropoikilitic nepheline. Small, subhedral grains (~1 mm) of titaniferous augite, amphibole, and calcium carbonate are also present in the nephelinite. Detailed descriptions of the volcanic unit and its contents have been previously reported (Dickey, 1968; Merrill and Wyllie, 1975; Corcoran and Moore, 2008). Recent ^{40}Ar–^{39}Ar dating of hornblende megacrysts from the KMB yielded an Upper Eocene age of 34.1 Ma (Hoernle et al., 2006), in general agreement with $^{87}Sr/^{86}Sr$ isotope dating of adjacent limestones (Nelson et al., 2004) and paleontological constraints from foraminifera in the overlying unit (Gage, 1965).

The polycrystalline amph-grt-cpx nodules are medium-grained (up to 4 mm grains but typically smaller) assemblages with xenomorphic granular to poikilitic textures where the amphibole commonly encloses the garnet and pyroxene grains (Dickey, 1968). The clinopyroxene within the polycrystalline amph-grt-cpx nodules exhibits weak lattice-preferred orientation as well as exsolution of garnet and orthopyroxene (Merrill and Wyllie, 1975). Lherzolite is the most common nodule in the KMB and has a xenomorphic granular texture with variable grain size (2–4 mm). The olivine in the lherzolite shows solid-state deformation indicated by strain bands and lattice-preferred orientation; the orthopyroxene exhibits distorted cleavage planes and exsolution laminae (Dickey, 1968). Reaction relationships between the nephelinite and lherzolite olivine and orthopyroxene yield clinopyroxene plus melt.

Compound polycrystalline nodules that include more than one of the nodule lithologies described above also occur in the KMB and demonstrate a pre-eruptive association of lherzolite with hornblendite and of lherzolite with the amph-grt-cpx lithology (Dickey, 1968). The most common compound nodules are fragments of deformed lherzolite that have been intruded or enveloped by undeformed polycrystalline hornblendite. The contact between the hornblendite and lherzolite is typically sharp and shows no reaction relationship. The contact association of lherzolite and the polycrystalline amph-grt-cpx was described by Dickey (1968), who observed a 1.5 cm band of amph-grt-cpx within lherzolite. No reaction relationship between the two was apparent, but amphibole was abundant within the amph-grt-cpx band that penetrated the lherzolite along grain boundaries near the contact. In addition, the garnet within the band was concentrated in a 2 mm strip parallel to the lherzolite contact.

The KMB megacrysts of garnet, clinopyroxene, and amphibole are distinct from the polycrystalline amph-grt-cpx nodules. The megacrysts occur almost exclusively as large single crystal fragments up to 8 cm. Rarely, bimineralic coarse aggregates of garnet and clinopyroxene are observed; hornblende megacrysts never form coarse aggregates with garnet or cpx megacrysts in the KMB (Dickey, 1968). No solid-state deformation or exsolution textures are present in the megacryst phases, in contrast with the polycrystalline amph-grt-cpx nodules (Merrill and Wyllie, 1975). The megacryst phases also have significantly higher Mg/Fe ratios and less compositional variation relative to the polycrystalline amph-grt-cpx nodules (Fig. 1).

From these observations, Dickey (1968) and Merrill and Wyllie (1975) both concluded that the lherzolite and polycrystalline amph-grt-cpx nodules represent pre-eruptive

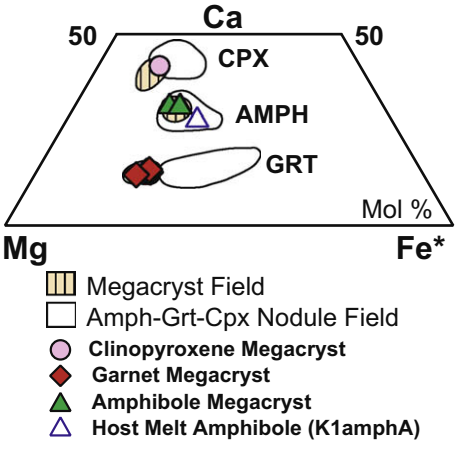

Fig. 1. The Ca–Fe*–Mg trends of KMB samples from this study, indicated by shaded symbols, and from previous studies, indicated the enclosed fields (Dickey, 1968; Mason, 1968; Zack et al., 1997). Fe* is total Fe. The megacrystic garnet and clinopyroxene plot in narrower compositional fields with higher Mg/Fe ratios than that garnet and cpx in the polycrystalline amph-grt-cpx nodules, while the megacrystic amphibole overlaps compositionally with the amphibole in the polycrystalline nodules.

basement rock into which the ascending nephelinite melt intruded. According to Merrill and Wyllie (1975), the polycrystalline amph-grt-cpx nodules represent a sequence of high-pressure cumulates from a fractionating magma different from that involved in the KMB eruption. The exsolution textures present in the clinopyroxene of the amph-grt-cpx nodules indicate that these nodules experienced low-temperature, high-pressure re-equilibration following crystallization. In contrast, the megacrysts of garnet, clinopyroxene, and amphibole display no evidence of solid-state deformation or low-temperature re-equilibration and must therefore have experienced histories different from the mixed nodules. Accordingly, Dickey (1968) and Merrill and Wyllie (1975) concluded that the megacrysts are likely cognate to the host magma, crystallized shortly before eruption, and were transported to the surface by the ascending nephelinite host melt.

These petrographic observations serve as the starting point for this partitioning study. While the majority of previous studies on the KMB focused on the polycrystalline amph-grt-cpx nodules (Mason, 1968; White et al., 1972; Zack et al., 1997), we have looked exclusively at the megacryst phases since only they can have a relevant cognate relationship with the KMB nephelinite host melt. Kakanui megacryst and nephelinite host melt samples were collected from exposures along the Kakanui beach and were chosen at random from well-spaced points along the outcrop spanning a distance of tens of meters. The samples were generally well-rounded but showed little evidence of alteration or metasomatism. Mineral and host melt samples were crushed into 0.5–1.0 mm diameter fragments with a piston press. Back scatter electron (BSE) images of representative garnet and amphibole megacryst samples show no significant compositional zonation, exsolution, or inhomogeneity (Fig. 2).

3. ANALYTICAL METHODS

Multiple crushed fragments (approximately 1.0 mm in size) of each hand specimen were randomly selected, set in an epoxy mount, polished, and carbon-coated. Major and minor element analyses of garnets and amphiboles were performed on the JEOL JXA-8800M electron microprobe at VU University Amsterdam. Analyses were performed with a focused beam using an acceleration voltage of 15 kV and a beam current of 25 nA. Natural and synthetic minerals were used as primary and secondary standards; calibrations were performed using the ZAF method.

Selected samples of garnet, amphibole, and host melt were analyzed for $^{176}Hf/^{177}Hf$ isotope compositions, Lu–Zr–Hf–Ta–W concentrations with isotope dilution, and Nb concentrations from Zr–Nb ratios (Münker et al., 2001; Weyer et al., 2002). Approximately 100 mg of crushed garnet megacryst (samples K2grtA, K2grtB, K6grtA, K7grtA, and K7grtB) and amphibole megacryst (samples K3amphA, K3amphB, K4amphA, and K4amphB) were hand picked under a microscope for mineral fragments that exhibited fresh cleavage on all surfaces. Duplicate analyses were performed on two garnet megacrysts (K2grt and K7grt) and two amphibole megacrysts (K3amph and K4amph). Approximately 150 mg of a crushed nephelinite clast were picked for the host melt sample (K1wrA). All visible calcite grains, which comprise <5% of the nephelinite clast by volume, were excluded from the sample as the calcite was assumed not to be a primary phase. A final sample of ~1 mm amphibole grains (hereafter "host melt amphibole", K1amphA) was separated from a different portion of the nephelinite host melt clast not used for sample K1wrA. The ~1 mm amphibole grains comprised approximately 5% of the nephelinite clast by volume and were selectively picked from the very fine-grained nephelinite groundmass to provide a compositional comparison with the amphibole megacrysts.

Sample table-top digestion was initiated with the addition of concentrated $HF:HNO_3$ (5:1) at 130 °C for several days. Samples were then dried down and taken up in ~7 M HCl + ~3 M HF at 130 °C. After addition of sufficient concentrated HNO_3 to remove fluorides, the samples were dissolved in 3 M HCl. Five percent aliquots (500 μL) were taken for trace element concentration determination, and the remaining solution volumes were spiked with a mixed ^{180}Ta–^{178}Hf–^{176}Lu–^{94}Zr tracer and a single ^{183}W tracer for isotopic dilution. Niobium concentrations were

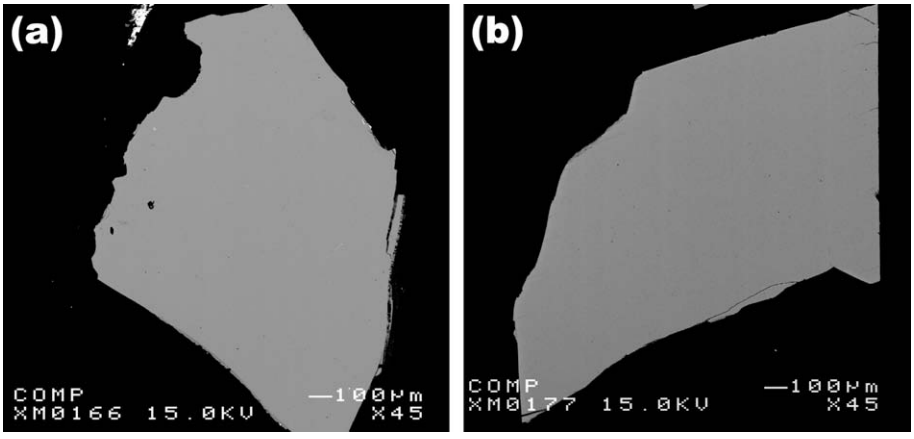

Fig. 2. Representative back scatter electron (BSE) images of KMB mineral fragments of (a) garnet and (b) amphibole. No significant compositional zonation or exsolution textures are visible. The two black spots on the garnet are dust on the surface of the mineral.

calculated from $^{91}Zr/^{93}Nb$ during Zr isotope measurements and Zr concentrations as obtained from the isotope dilution results. The full analytical procedure for HFSE + Lu separation and analysis, including the determination of Nb concentrations from Zr/Nb ratios, has been described in detail elsewhere (Münker et al., 2001; Weyer et al., 2002; Nebel et al., 2009). Briefly, a two column-three stage procedure with Eichrom Ln-resin and conventional anion-resin was used to separate Lu and HFSE from the sample matrix. The final separates included purified Zr–Nb–W, Ta, Hf, and a Lu-rich HREE fraction, all of which were analyzed with a Thermo-Finnigan Neptune MC-ICP-MS (VU University Amsterdam). Typical reproducibility for the isotope dilution concentrations are ~0.1% for Hf, Lu, Zr, 1% for Ta and W, and 5% for mono-isotopic Nb (Weyer et al., 2002; Nebel et al., 2009). Isotope composition (IC) analyses of Hf follow procedures outlined previously (Morel et al., 2008). All isotope compositions are reported relative to a JMC-475 reference value of $^{176}Hf/^{177}Hf = 0.282160$ (Blichert-Toft et al., 1997) and are expressed in the ε_{Hf} notation, defined as the deviation from the chondritic uniform reservoir multiplied by 10,000 (Blichert-Toft and Albarède, 1997; Bouvier et al., 2008). Procedural blanks are Zr = 125 pg, Hf = 15 pg, Nb = 90 pg, Ta = 10 pg, and Lu = 30 pg. Isochron relationships are calculated using IsoPlot (Ludwig, 2001) and the external reproducibility of our measurements are ±0.2% for the Lu/Hf and ±0.000014 for the $^{176}Hf/^{177}Hf$, as determined by multiple analyses of standard reference materials and solutions (e.g., Morel et al., 2008; Nebel et al., 2009).

A full set of sample trace element concentrations were determined with a Thermo X-Series II ICP-MS (VU University Amsterdam). Samples were prepared by diluting the five percent aliquots to ~1:5000 with a 5% HNO_3 solution. Standard operating procedures were used on the ICP-MS and concentrations of forty-five trace elements were measured. Instrumental drift and external reproducibility were controlled using in-house calibrants and BHVO-2 and BCR-2 reference materials.

4. RESULTS

4.1. Major element variation/electron microprobe results

The KMB megacrysts are all characterized by highly uniform composition and appearance (Fig. 2). No compositional zonation or exsolution textures were observed in any of the studied mineral phases, in agreement with the petrographic observations of Dickey (1968) and Merrill and Wyllie (1975). Mineral inclusions were also not observed within any of the samples to within the resolution of back scatter electron (BSE) images (~0.5 μm).

Major and minor element compositions for the KMB garnet, amphibole, and clinopyroxene megacrysts and host melt amphibole (Table 1 and Fig. 1) are highly uniform for each hand specimen. The compositional differences of numerous fragments derived from the each hand specimen do not exceed instrumental uncertainty (Table 1; measurement 2σ <0.9 wt% for all major elements and is more typically <0.3 wt%). The garnet megacrysts are pyrope-rich

Table 1
Major element composition as determined by electron microprobe (wt%). FeO* is total iron and *N* is number of analyses.

Oxide	Clast 1		Clast 3		Clast 4		Clast 10		Clast 2		Clast 5		Clast 6		Clast 7		Clast 8		Clast 5	
	K1amph[a]	2sd	K3amph[b]	2sd	K4amph[b]	2sd	K10amph[b]	2sd	K2grt	2sd	K5grt	2sd	K6grt	2sd	K7grt	2sd	K8grt	2sd	K5cpx	2sd
SiO_2	40.31	0.34	39.10	0.17	38.72	0.37	38.88	0.28	41.14	0.58	40.74	0.33	40.71	–	41.29	0.57	41.73	0.59	49.0	0.26
TiO_2	4.72	0.10	3.65	0.07	3.71	0.06	3.71	0.04	0.56	0.05	0.47	0.07	0.52	–	0.57	0.06	0.47	0.04	1.5	0.01
Al_2O_3	13.53	0.15	14.06	0.32	13.74	0.18	13.83	0.32	23.01	0.53	22.68	0.50	22.22	–	23.11	0.43	23.36	0.27	9.3	0.27
Cr_2O_3	0.00	0.00	0.00	0.00	0.00	0.00	0.00	0.00	0.00	0.00	0.00	0.00	0.00	–	0.00	0.00	0.00	0.00	0.0	0.00
FeO*	13.09	0.29	10.25	0.93	11.39	0.32	11.53	0.15	12.47	0.62	12.49	0.38	12.11	–	12.54	0.38	11.50	0.12	7.3	0.22
MnO	0.06	0.08	0.06	0.07	0.12	0.05	0.03	0.05	0.30	0.12	0.32	0.05	0.37	–	0.31	0.08	0.30	0.12	0.1	0.07
MgO	11.05	0.11	13.31	0.56	12.52	0.18	12.61	0.16	16.73	0.33	16.67	0.08	16.86	–	16.91	0.09	18.10	0.19	13.3	0.33
CaO	9.87	0.11	12.10	0.14	12.01	0.08	12.05	0.11	5.64	0.16	5.38	0.14	5.49	–	5.70	0.08	5.24	0.07	17.2	0.10
Na_2O	2.96	0.08	1.98	0.08	1.97	0.05	2.02	0.04	0.03	0.01	0.03	0.02	0.02	–	0.03	0.01	0.03	0.01	1.8	0.03
K_2O	2.03	0.03	2.40	0.11	2.47	0.05	2.42	0.04	–	–	–	–	–	–	–	–	–	–	–	–
F	0.08	0.07	0.10	0.08	0.10	0.07	0.09	0.07	–	–	–	–	–	–	–	–	–	–	–	–
Cl	0.02	0.01	0.02	0.01	0.02	0.01	0.01	0.01	–	–	–	–	–	–	–	–	–	–	–	–
Total	97.72	0.21	97.02	0.50	96.77	0.33	97.20	0.51	99.88	1.70	98.76	0.87	98.30	–	100.45	1.07	100.72	0.72	99.4	0.82
N	8		11		7		7		9		5		1		7		6		3	

[a] Amphibole crystals (~1 mm^3) sampled from nephelinite host melt clast.
[b] Amphibole megacryst clasts.

with minor variation in MgO, FeO* (total iron), and CaO content. The average garnet composition observed in these samples expressed as aluminosilicate garnet end members pyrope [Py ($Mg_3Al_2Si_3O_{12}$)], almandine [Alm ($Fe_3Al_2Si_3O_{12}$)], spessartine [Sp ($Mn_3Al_2Si_3O_{12}$)], and grossular [Gr ($Ca_3Al_2Si_3O_{12}$)] is $Py_{61}Alm_{24}Sp_1Gr_{14}$. Titanium oxide content is low at ~0.5 wt%. The KMB garnet megacrysts overlap compositionally with garnets found in mantle peridotites, pyroxenites, and calcium-poor Group A eclogites (van Westrenen et al., 2001a; references therein). The KMB amphibole megacrysts are titanian pargasite (Leake et al., 1997) and are very uniform in composition. The host melt amphibole (K1amphA) is kaersutite, highly uniform, and has a distinct composition from the megacrysts with relative enrichments in SiO_2, TiO_2, Na_2O, and FeO* and depletions in CaO, MgO, and K_2O. The compositions of both amphiboles fall within the wider range previously reported for KMB (Fig. 1; see also Dickey, 1968; Mason, 1968; Zack et al., 1997). Clinopyroxene from Clast 5, a garnet-clinopyroxene bimineralic coarse aggregate (see Section 2 – Petrography) has a significant Ca-Tschermaks ($CaAlAlSiO_6$) component typical for the KMB.

4.2. Isotope dilution concentrations of Zr, Hf, Ta, Lu, and W

Eleven samples were analyzed for Zr, Hf, Ta, Lu, and W concentrations with isotope dilution (Table 2). The garnet megacrysts have a high level of compositional uniformity. Zirconium and Hf concentrations between the different garnet samples have relative standard deviations (RSD) of less than 3%. The largest variation in the garnet megacrysts occurs for Ta, which is likely due to the very low concentrations of <10 ppb measured in the garnet that approach the limits of detection for the isotope dilution method. The KMB amphibole megacrysts are also compositionally uniform with HFSE concentration RSDs less than 5%. The host melt amphibole contains lower concentrations of Zr, Hf, Ta, and Lu and higher W than the amphibole megacrysts, showing that these two phases are distinct for both the major and trace element compositions. The nephelinite host melt has the highest HFSE concentrations of the phases studied.

Significant differences in HFSE ratios occur between the different KMB phases (Table 2). Garnet and the nephelinite samples exhibit super-chondritic Zr/Hf ~ 50, whereas amphibole shows sub-chondritic ratios of ~25 (chondrite Zr/Hf = 34.3 ± 0.3, Münker et al., 2003). The garnet and amphibole samples all have sub-chondritic Nb/Ta values, while the KMB nephelinite shows super-chondritic Nb/Ta = 22.2 (chondrite Nb/Ta = 19.9 ± 0.6, Münker et al., 2003). The garnet Nb/Ta ratios have the largest range, likely due to the very low Ta concentrations in garnet that approach the lower limits of detection for our method.

4.3. Lu–Hf isotopic data

The $^{176}Lu/^{177}Hf$ and $^{176}Hf/^{177}Hf$ isotope compositions (Table 3 and Fig. 3) were determined for the same eleven samples analyzed for HFSE concentrations. Garnet megacrysts are uniform with mean $^{176}Lu/^{177}Hf = 0.111 \pm 0.009$ (2σ) and $^{176}Hf/^{177}Hf = 0.282964 \pm 0.000019$. The nephelinite and host melt amphibole have $^{176}Hf/^{177}Hf = 0.282925 \pm 0.000014$ and 0.292908 ± 0.000014, respectively, which are in general agreement with Hf isotope composition measurements of other monogenetic Waiareka–Deborah Volcanic Units in the region ($^{176}Hf/^{177}Hf = 0.282905 \pm 0.000008$ and 0.282899 ± 0.000007) from Timm et al. (2010). The Lu–Hf data for the garnet megacrysts, nephelinite, and host melt amphibole form an isochron relationship that yields a MSWD = 1.7 and an average initial $^{176}Hf/^{177}Hf = 0.282915 \pm 0.000010$. The amphibole megacrysts have indistinguishable Lu/Hf and Hf isotopic compositions to within error [$^{176}Lu/^{177}Hf = 0.00216 \pm 0.00016$ (2σ) and $^{176}Hf/^{177}Hf = 0.282832 \pm 0.000011$], but plot significantly below the isochron relationship defined by the garnet megacrysts, nephelinite, and host melt amphibole (Fig. 3).

A high-precision eruption age of the Kakanui volcanics has been determined by ^{40}Ar–^{39}Ar dating on KMB hornblende megacryst and yields an age of 34.1 ± 0.1 Ma (Hoernle et al., 2006). A reference isochron with this ^{40}Ar–^{39}Ar eruption age for the KMB plots through the Lu–Hf isotopic data for the garnet megacrysts, nephelinite, and host melt

Table 2
Lu–Hf–Zr–Ta–W(–Nb) isotope dilution concentrations for garnet megacrysts, amphibole megacrysts, host melt amphibole (K1amphA), and nephelinite (K1wrA). Typical reproducibility is ~0.1% for Hf, Lu, Zr; 1% for Ta and W; and 5% for Nb. Nb concentrations determined from Zr–Nb ratios (see text). Note that multiple mineral separates were sometimes sampled from a single clast to assess trace element heterogeneity (e.g., K2grtA and K2grtB were sampled from the same hand specimen, Clast 2–K2grt in Table 1).

Sample	Lu (ppm)	Hf (ppm)	Zr (ppm)	Nb (ppm)	Ta (ppm)	W (ppm)	Lu/Hf	Zr/Nb	Nb/Ta	Zr/Hf	Hf/W
K2grtA	1.262	1.561	78.78	0.087	0.006	0.012	0.8081	906	14.0	50.46	134
K2grtB	1.197	1.581	79.82	0.086	0.008	0.013	0.7567	933	10.6	50.48	126
K6grtA	1.280	1.583	80.01	0.097	0.005	0.013	0.8086	828	18.6	50.55	121
K7grtA	1.314	1.594	80.57	0.098	0.006	0.013	0.8246	822	16.8	50.55	126
K7grtB	1.299	1.548	77.54	0.094	0.010	0.010	0.8391	828	9.63	50.08	154
K1amphA	0.046	3.319	82.33	31.1	1.66	0.072	0.01378	2.65	18.7	24.81	46.3
K3amphA	0.109	6.708	154.5	30.3	1.89	0.019	0.01621	5.10	16.0	23.03	346
K3amphB	0.108	6.604	154.0	30.2	1.88	0.055	0.01629	5.10	16.1	23.32	121
K4amphA	0.104	6.830	159.2	32.4	1.98	0.015	0.01529	4.91	16.4	23.31	459
K4amphB	0.100	6.554	155.6	29.6	1.88	0.013	0.01526	5.25	15.8	23.74	518
K1wrA	0.165	7.278	361.4	139	6.25	0.961	0.02266	2.61	22.2	49.66	7.57

Table 3
Hafnium isotope compositions determined by MC-ICP-MS. The typical reproducibility on $^{176}Hf/^{177}Hf$ is ±0.000014 (2σ), corresponding to ±0.5 ε_{Hf}. The epsilon notation is deviation from the chondritic uniform reservoir multiplied by 10,000 (Blichert-Toft and Albarède, 1997). The Lu decay constant used is $\lambda^{176}Lu = 1.865 \pm 0.015 \times 10^{-11}$ year^{-1} (Scherer et al., 2001; Söderlund et al., 2004).

Sample	$^{176}Lu/^{177}Hf$	$^{176}Hf/^{177}Hf$	±2se (6th digit)	ε_{Hf}	$^{176}Hf/^{177}Hf$ initial ($T = 34.1$ Ma)	ε_{Hf} initial ($T = 34.1$ Ma)
K2grtA	0.1109	0.282961	6	+6.7	0.282890	+4.9
K2grtB	0.1038	0.282953	4	+6.4	0.282888	+4.8
K6grtA	0.1109	0.282957	5	+6.5	0.282887	+4.8
K7grtA	0.1131	0.282972	5	+7.1	0.282900	+5.3
K7grtB	0.1151	0.282976	5	+7.2	0.282903	+5.4
K1amphA	0.001890	0.282908	5	+4.8	0.282906	+5.5
K3amphA	0.002224	0.282825	5	+1.9	0.282824	+2.6
K3amphB	0.002235	0.282831	3	+2.1	0.282830	+2.8
K4amphA	0.002098	0.282839	4	+2.4	0.282837	+3.1
K4amphB	0.002093	0.282832	5	+2.1	0.282831	+2.8
K1wrA	0.003108	0.282925	4	+5.4	0.282923	+6.1

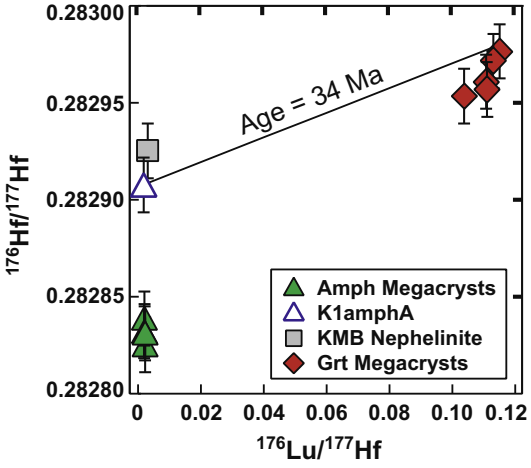

Fig. 3. Lu–Hf isotope evolution diagram of the Kakanui Mineral Breccia (KMB) megacryst and nephelinite samples. A reference isochron with the ^{40}Ar–^{39}Ar apparent eruption age of 34.1 Ma for the KMB (Hoernle et al., 2006) is plotted with the data. Note that the KMB amphibole megacryst samples plot significantly below the trend defined by the other samples.

amphibole in the Lu–Hf isochron diagram (Fig. 3). In contrast, the KMB amphibole megacrysts plot below the reference isochron with significantly lower Hf isotope compositions. This observation along with the associated small MSDW of the afore mentioned phases is strongly supportive that mineral–melt isotope equilibration was achieved at the time of formation for the garnet megacrysts, nephelinite, and host melt amphibole. The amphibole megacryst isotope compositions, however, suggests the involvement of a distinct melt source for these crystals that contained a stronger non-radiogenic signature than the KMB nephelinite.

4.4. ICP-MS trace element data

The samples were analyzed for 45 trace element concentrations using a single-collector-ICP-MS (Table 4 and Fig. 4).

Garnet. The trace element concentrations of the garnet megacrysts are highly consistent and duplicate sample runs are indistinguishable within error. The garnets are generally depleted in LREE relative to HREE, although extreme HREE enrichment is not observed [$(Ho/Lu)_N \sim 1$]. The LREE (notably La, Ce, and Pr) also display appreciable enrichment relative to the general REE trend. The highly incompatible LILE (Cs, Rb, Ba) content measured in these megacrysts is comparable with concentrations found in garnets of the polycrystalline amph-grt-cpx nodules (Zack et al., 1997).

Amphibole. The amphibole megacryst trace element concentrations are indistinguishable to within error but differ significantly from the host melt amphibole, in agreement with the major element and Hf isotopic trends. The amphibole megacrysts have consistently higher concentrations of REE than the host melt amphibole, notably for the LREE.

Host melt. The nephelinite host melt shows a considerable LREE-enriched REE trend. Chondrite-normalized LREE concentrations are greater than ten times higher in the host melt than the HREE. Hoernle et al. (2006) previously studied the Kakanui mela-nephelinite with XRF and ICP-MS and observed trace element trends very similar to our results. The overall heterogeneity of the nephelinite appears to be comparably small for the fluid immobile HREE and HFSE as differences between the two analyses do not exceed a factor of 1.4. Hoernle et al. (2006) consistently measured higher concentrations for the fluid-mobile LILE and LREE, but the differences still do not exceed a factor of 3.

4.5. Isotope dilution MC-ICP-MS vs. ICP-MS analyses

A comparison of the HSFE concentrations as determined by isotope dilution (ID) and single-collector-ICP-MS is shown in Fig. 5. All concentrations determined for Zr, Hf, and Lu in all mineral phases plot on the 1:1 line, and Nb and Ta concentrations in the amphibole and nephelinite have similar levels of agreement. Niobium and Ta concentrations in the garnet megacrysts and W concentrations in all megacrysts show significant disagreement between the two methods, with the ID concentrations being

Table 4
Trace element compositions as determined by single-collector-ICP-MS (ppm).

Element	K2grtA	K2grtB	K6grtA	K7grtA	K7grtB	K1amphA	K3amphA	K3amphB	K4amphA	K4amphB	K1wrA
Li	0.50	0.64	0.68	0.49	0.46	2.48	3.13	0.94	0.95	1.04	73.79
Be	0.02	0.04	0.00	0.00	0.01	0.61	0.45	0.42	0.49	0.59	1.85
Sc	103.7	91.54	102.8	103.8	106.7	14.78	83.36	81.77	56.60	57.65	19.73
Ti	3987	3767	3830	3750	3814	30,423	23,332	23,275	23,743	23,224	20,740
V	201.9	187.7	195.1	190.6	189.3	348.4	348.7	345.8	381.7	375.5	209.6
Cr	86.7	75.2	102.9	94.0	79.6	26.70	43.17	47.67	46.17	40.92	197.81
Co	72.90	67.85	67.76	67.25	69.55	76.85	56.83	56.31	57.57	56.74	53.30
Ni	57.48	50.36	54.66	54.02	58.02	31.10	121.21	118.05	80.63	85.01	121.32
Cu	3.47	3.55	3.59	3.35	3.47	25.01	20.65	20.78	19.13	21.14	44.12
Zn	66.1	61.2	58.7	53.5	53.2	109.6	76.0	71.6	82.5	100.0	182.2
Ga	8.78	8.31	8.18	8.34	8.38	22.99	16.74	16.76	17.33	17.23	19.12
Rb	2.66	2.49	2.67	1.84	1.82	17.59	14.57	14.69	15.86	16.41	20.74
Sr	14.12	13.36	13.55	8.11	8.54	525.1	731.5	724.9	643.1	628.2	456.3
Y	89.9	82.5	86.1	85.9	88.6	11.76	14.99	14.69	14.07	13.59	22.82
Zr	96.4	89.0	93.7	91.5	92.0	93.4	172.1	170.5	181.2	177.4	388.4
Nb	0.18	0.19	0.21	0.16	0.17	30.88	30.96	30.28	32.00	30.40	138.77
Mo	0.006	0.009	0.009	0.006	0.009	0.025	0.008	0.005	0.008	0.011	0.88
Cd	0.10	0.11	0.10	0.08	0.13	0.08	0.08	0.07	0.06	0.12	0.16
In	0.19	0.18	0.17	0.15	0.17	0.17	0.26	0.26	0.24	0.22	0.18
Sn	0.08	0.01	0.06	0.00	0.03	0.85	1.68	1.66	1.57	1.53	1.21
Sb	0.01	0.01	0.01	0.00	0.02	0.01	0.00	0.01	0.00	0.01	0.05
Cs	0.09	0.08	0.07	0.05	0.05	0.06	0.13	0.13	0.05	0.11	0.44
Ba	6.85	7.13	7.32	4.81	4.79	275.5	466.2	462.1	470.0	467.2	276.6
La	0.46	0.44	0.42	0.30	0.30	5.81	13.75	13.69	12.00	11.57	36.52
Ce	0.87	0.88	0.87	0.66	0.66	19.61	43.31	43.02	38.98	37.39	83.58
Pr	0.20	0.19	0.19	0.17	0.18	3.44	7.01	6.94	6.44	6.13	10.60
Nd	1.94	1.82	1.89	1.72	1.83	18.49	33.82	33.55	31.53	30.29	44.96
Sm	2.03	1.94	1.93	1.92	2.00	4.92	7.06	6.95	6.65	6.52	8.92
Eu	1.19	1.12	1.19	1.21	1.23	1.76	2.17	2.11	2.07	2.03	2.96
Gd	5.83	5.67	5.80	5.49	5.73	4.67	5.66	5.53	5.37	5.24	7.50
Tb	1.48	1.40	1.43	1.39	1.47	0.63	0.70	0.70	0.68	0.68	1.04
Dy	11.93	11.37	11.61	11.51	11.82	2.90	3.40	3.33	3.26	3.24	5.03
Ho	2.98	2.79	2.93	2.89	3.01	0.44	0.55	0.55	0.53	0.51	0.83
Er	9.62	8.99	9.71	9.75	9.77	0.90	1.30	1.32	1.20	1.18	1.97
Tm	1.38	1.26	1.36	1.38	1.42	0.09	0.14	0.15	0.14	0.14	0.22
Yb	9.16	8.40	9.10	9.01	9.14	0.40	0.81	0.83	0.78	0.81	1.30
Lu	1.37	1.23	1.42	1.45	1.43	0.05	0.11	0.11	0.11	0.11	0.19
Hf	1.71	1.73	1.64	1.65	1.61	3.33	6.67	6.51	6.83	6.64	7.43
Ta	0.18	0.08	0.13	0.11	0.06	2.03	2.35	2.32	2.43	2.37	7.56
W	0.205	0.181	0.192	0.190	0.188	0.104	0.048	0.044	0.052	0.038	1.018
Tl	0.033	0.028	0.025	0.017	0.015	0.054	0.073	0.070	0.082	0.073	0.070
Pb	0.020	0.026	0.025	0.062	0.047	0.198	0.365	0.386	0.350	0.339	2.809
Bi	0.022	0.004	0.001	0.001	0.002	0.001	0.003	0.002	0.003	0.002	0.020
Th	0.089	0.086	0.088	0.060	0.060	0.101	0.216	0.225	0.171	0.196	4.326
U	0.010	0.009	0.010	0.009	0.010	0.020	0.021	0.019	0.014	0.018	0.938

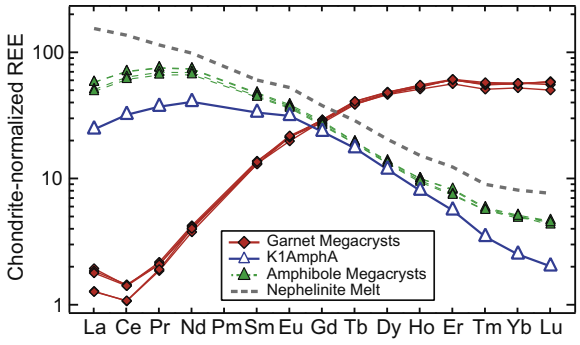

Fig. 4. Chondrite-normalized rare earth element concentrations for the KMB garnet, amphibole, and nephelinite (normalization to chondrite data of McDonough and Sun, 1995). The five garnet megacryst and four amphibole megacryst samples each have highly uniform REE concentrations. The host melt amphibole (K1amphA) is less enriched in REE than the amphibole megacrysts.

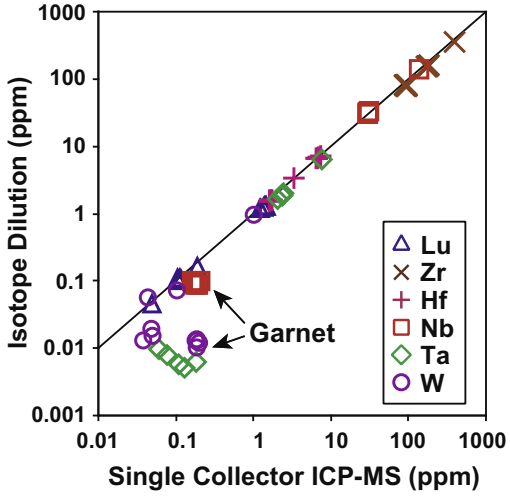

Fig. 5. A comparison of HFSE and Lu concentrations (ppm) as determined by isotope dilution (MC-ICP-MS) and single-collector-ICP-MS. Although most measurements show excellent agreement, the W, Ta, and Nb concentrations for garnet are overestimated by ICP-MS relative to isotope dilution.

consistently lower than those determined by single-collector-ICP-MS. The difference is especially significant (up to two orders of magnitude) for Ta and W. In the case of the Ta ID measurements, it is difficult to envision scenarios where (a) sample-spike equilibrium is reached only with the amphibole and nephelinite samples but not the garnet, or (b) that Ta is lost selectively from only the garnet samples (and not the amphibole or nephelinite) before loading onto the columns, but the Ta spike is selectively retained. Since Nb and Ta in garnet and W in all silicate minerals occur in very low absolute concentrations, our data show that the higher precision and accuracy afforded by ID MC-ICP-MS may allow for more realistic constraints of $HFSE^{5+}$ and W concentrations in silicate minerals in the lower ppb range.

4.6. Trace element partitioning

Garnet. Garnet–host melt partition coefficients ($D^{Grt/L}$) derived from both the isotope dilution MC-ICP-MS and single-collector-ICP-MS data sets (Table 5) are plotted with previously reported experimentally determined $D^{Grt/L}$ values from a wide range of pressures and temperatures, melt water contents, and melt compositions (Fig. 6a). The full range of experimental data applies to garnet participation in magmatic differentiation in the deep mantle, mid-ocean ridges, and subduction zones (for references, see Fig. 6).

The most immediate results of this study are the very small absolute values determined for D_{Nb} and D_{Ta} in garnet – up to three orders of magnitude smaller than literature values shown in Fig. 6a. The high precision isotope dilution concentrations of Nb and Ta in garnet are very low, with all Ta concentrations less than 10 ppb. The higher $D^{Grt/L}$ values reported elsewhere could very well be due to overestimation of $HFSE^{5+}$ contents in mineral phases, especially for Ta, when using traditional in situ methods. In addition to analytical difficulties related to the poor ionization properties of the HFSE, it is extremely difficult to fully exclude the presence of very small melt inclusions in experimentally grown minerals. The presence of even minute percentages of such inclusions can significantly affect the resulting measured D values for highly incompatible elements (van Westrenen et al., 2001b). We suggest that the long time scales of natural mineral growth compared to experimental conditions may allow for the formation of inclusion-free phases, allowing for more accurate D measurements for highly incompatible elements.

The average D_{Nb}/D_{Ta} of the megacryst garnets (0.6 ± 0.3) is in general agreement with values reported for a wide range of P–T-composition conditions by others, i.e., Klimm et al. (2008) (0.72 ± 0.04, $X_{grossular} = 24 \pm 2$ mol%, $T = 800$–900 °C) and Pertermann et al. (2004) (0.58 ± 0.09, $X_{grossular} = 18$–25%, $T = 1325$–1350 °C). This agreement is notable given that the KMB garnet megacrysts contain lower grossular content ($X_{grossular} = 14\%$) but formed at an intermediate temperature (see Section 5.1; also Merrill and Wyllie, 1975). In contrast, the D_{Nb}/D_{Ta} values reported by Green et al. (2000) and Zack et al. (1997) are significantly lower, due primarily to D_{Ta} values that are orders of magnitude larger than D_{Nb}. Given the low concentrations of Ta that we observe in KMB megacrystic garnet and the similarity of the Nb and Ta ionic radii, we suggest this discrepancy could be due to difficulties in Ta concentration determinations.

Assembly of a set of the most recent Zr and Hf garnet partition coefficients (for references, see Fig. 6) shows that garnet D_{Zr} and D_{Hf} display moderate inverse correlation to grossular content and temperature as discussed by van Westrenen et al. (2001a) and Klimm et al. (2008). Zirconium and Hf become compatible in garnets roughly when grossular content exceeds ~24% (van Westrenen et al., 2001a) or formation temperatures fall below ~950 °C. D_{Zr} and D_{Hf} greatly increase for the low T experiments of Klimm et al. (2008) ($T = 800$–900 °C) and Green and Adam (2003) ($T = 700$ °C), suggesting a nonlinear temperature dependence. The assembled data set also shows no significant

Table 5
Mineral–melt partition coefficients.

Element	K1amphA D(Amp/L)	K2grtA D(Grt/L)	K2grtB D(Grt/L)	K6grtA D(Grt/L)	K7grtA D(Grt/L)	K7grtB D(Grt/L)	Avg Grt D(Grt/L)	±2σ
Li	0.03	0.007	0.009	0.009	0.007	0.006	0.008	0.003
Be	0.33	0.012	0.021	0.000	0.000	0.005	0.007	0.017
Sc	0.75	5.3	4.6	5.2	5.3	5.4	5.2	0.6
Ti	1.47	0.192	0.182	0.185	0.181	0.184	0.185	0.009
V	1.66	0.96	0.90	0.93	0.91	0.90	0.92	0.05
Cr	0.13	0.44	0.38	0.52	0.48	0.40	0.44	0.11
Co	1.44	1.37	1.27	1.27	1.26	1.30	1.30	0.09
Ni	0.26	0.47	0.42	0.45	0.45	0.48	0.45	0.05
Cu	0.57	0.08	0.08	0.08	0.08	0.08	0.08	0.00
Zn	0.60	0.36	0.34	0.32	0.29	0.29	0.32	0.06
Ga	1.20	0.46	0.43	0.43	0.44	0.44	0.44	0.02
Rb	0.85	0.13	0.12	0.13	0.09	0.09	0.11	0.04
Sr	1.15	0.031	0.029	0.030	0.018	0.019	0.025	0.013
Y	0.52	3.9	3.6	3.8	3.8	3.9	3.8	0.2
Zr[a]	0.228	0.218	0.221	0.221	0.223	0.215	0.220	0.007
Nb[a]	0.22	0.0006	0.0006	0.0007	0.0007	0.0007	0.0007	0.0001
Mo	0.03	0.007	0.010	0.010	0.007	0.010	0.009	0.003
Sn	0.71	0.06	0.01	0.05	0.00	0.03	0.03	0.05
Cs	0.14	0.21	0.18	0.16	0.12	0.12	0.16	0.08
Ba	1.00	0.025	0.026	0.026	0.017	0.017	0.022	0.009
La	0.16	0.013	0.012	0.012	0.008	0.008	0.011	0.004
Ce	0.23	0.010	0.011	0.010	0.008	0.008	0.009	0.003
Pr	0.32	0.019	0.018	0.018	0.016	0.017	0.018	0.002
Nd	0.41	0.043	0.040	0.042	0.038	0.041	0.041	0.004
Sm	0.55	0.228	0.218	0.217	0.216	0.225	0.221	0.011
Eu	0.60	0.40	0.38	0.40	0.41	0.41	0.40	0.03
Gd	0.62	0.78	0.76	0.77	0.73	0.76	0.76	0.04
Tb	0.61	1.42	1.35	1.38	1.34	1.42	1.38	0.07
Dy	0.58	2.37	2.26	2.31	2.29	2.35	2.32	0.09
Ho	0.53	3.58	3.36	3.52	3.48	3.62	3.51	0.21
Er	0.45	4.9	4.6	4.9	4.9	5.0	4.9	0.3
Tm	0.38	6.2	5.7	6.1	6.2	6.4	6.1	0.6
Yb	0.31	7.0	6.5	7.0	6.9	7.0	6.9	0.5
Lu[a]	0.28	7.6	7.3	7.8	8.0	7.9	7.7	0.6
Hf[a]	0.456	0.215	0.217	0.217	0.219	0.213	0.216	0.005
Ta[a]	0.27	0.0010	0.0013	0.0008	0.0009	0.0016	0.0011	0.0006
W[a]	0.075	0.0121	0.0130	0.0136	0.0131	0.0105	0.0125	0.0025
Tl	0.77	0.5	0.4	0.4	0.2	0.2	0.3	0.2
Pb	0.071	0.007	0.009	0.009	0.022	0.017	0.013	0.013
Th	0.023	0.021	0.020	0.020	0.014	0.014	0.018	0.007
U	0.022	0.011	0.010	0.011	0.009	0.011	0.010	0.002

[a] Partition coefficients for Zr, Lu, Hf, Ta, and W determined from isotope dilution with MC-ICP-MS. Nb concentration determined from Zr–Nb ratios (see Section 3). All other element partition coefficients determined with ICP-MS.

correlation of Zr and Hf partitioning with TiO_2 content in garnet, in contrast to Pertermann et al. (2004). The KMB megacrystic garnet $HFSE^{4+}$ partition coefficients from this study fit into the greater literature trends. The megacrystic garnet D_{Zr}/D_{Hf} ratios show excellent agreement [1.015 ± 0.008 (2σ)]. From the assembled data set, garnet D_{Zr}/D_{Hf} ratios generally increase for lower T and higher grossular content garnets. Accordingly, Klimm et al. (2008) observed significantly larger D_{Zr}/D_{Hf} values of 3.11 ± 0.18 (mean grossular content of 24 ± 2 mol%), which may be explained by preferential partitioning of Zr into the dodecahedral X site relative to Hf (van Westrenen et al., 2001a).

The KMB megacrystic garnet D_W values are in excellent agreement with each other, with a mean of 0.0125 ± 0.0025, despite the low absolute abundances. Very few experimental studies have previously investigated W partitioning in garnet due to the extremely low tungsten concentrations involved. Righter and Shearer (2003) and Adam and Green (2006) both observed D_W values from 0.01 to 0.0007, but no correlation with temperature or garnet composition is apparent. D_{Hf}/D_W ratios for KMB megacrystic garnets (17 ± 3) plot at the lower limit of previous results ($D_{Hf}/D_W = 20$–173).

The mean of D_U/D_{Th} for KMB garnet megacrysts is 0.59 ± 0.24, which is in agreement with Klimm et al. (2008) but is considerably lower than most other experimental partitioning studies. The difference is likely due to the higher oxygen fugacity (fO_2) in the systems of this study and Klimm et al. (2008), resulting in elevated U^{5+} and U^{6+} oxidation states that are much less compatible in garnet

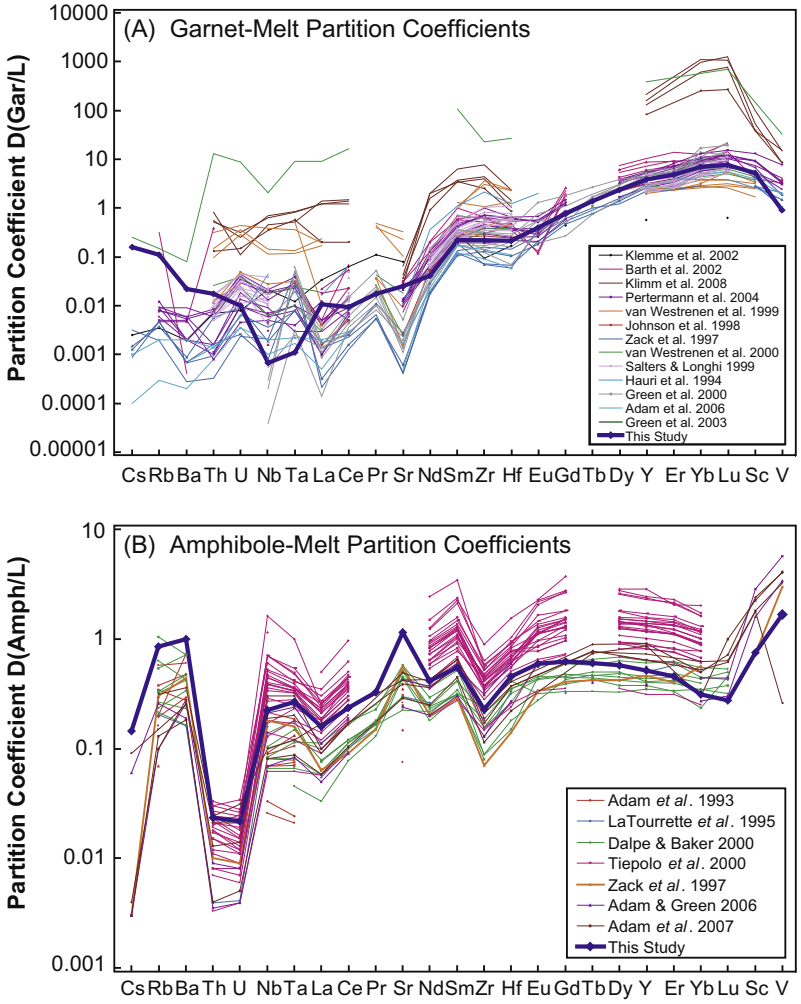

Fig. 6. Mineral–melt partition coefficients for (a) garnet and (b) amphibole. The newly determined partition coefficients from this study plotted with the heavily weighted line. Other garnet partition coefficients (Hauri et al., 1994; Zack et al., 1997; Johnson, 1998; Salters and Longhi, 1999; van Westrenen et al., 1999, 2000; Green et al., 2000; Barth et al., 2002; Klemme et al., 2002; Green and Adam, 2003; Pertermann et al., 2004; Adam and Green, 2006; Klimm et al., 2008) and amphibole partition coefficients (Adam et al., 1993, 2007; LaTourrette et al., 1995; Zack et al., 1997; Dalpé and Baker, 2000; Tiepolo et al., 2000a,b, 2001; Adam and Green, 2006) are plotted for comparison.

than U^{4+}. In highly oxidizing magmatic systems including subduction zones and alkali volcanism similar to KMB nephelinite, Th is therefore preferentially incorporated into garnet relative to U, resulting in U/Th fractionation that is opposite of the drier, lower fO_2 conditions of mid-ocean ridge magmatism. Thus, although U and Th partitioning between garnet and anhydrous melt display similar behavior to $HFSE^{4+}$, D_U also has a clear fO_2 dependence that should be considered in modeling of, for example, the effect of residual garnet on the development of U–Th disequilibrium in magma. This fO_2 dependence can also lead to a decoupling of the generally well correlated elements U and W, whereas Th/W should not be affected by fO_2.

Middle and heavy rare earth element partition coefficients for the KMB garnet megacrysts show excellent agreement with high-pressure experiments at similar temperature. D_{LREE}, notably for La and Ce, are larger than expected, and all D_{LILE} (Cs, Rb, Ba, Sr) derived from KMB garnets are higher than observed in Pertermann et al. (2004), Adam and Green (2006), and Barth et al. (2002). The D_{LREE} differences cannot be explained by host melt heterogeneity since the LILE concentrations measured by Hoernle et al. (2006) differ by less than a factor of 3 from our measurements on a different KMB host melt sample. Since LREE and LILE concentrations in garnet are expected to be very low, sub-micron-sized fluid inclusions rich in fluid-mobile elements could be a plausible explanation for the higher than expected partitioning values. Alternatively, selective loss of a volumetrically minor fluid-rich phase from the host melt during eruption could lead to significant overestimation of mineral–melt partition coefficients for fluid-mobile elements. We therefore view the D_{LREE} and D_{LILE} values with caution.

Amphibole. Partition coefficients $D^{Amph/L}$ for the KMB host melt amphibole and also between titanian pargasite and kaersutite amphiboles and their respective silica-poor host melts (picrites, basanites, and nephelinites) from previous studies are plotted in Fig. 6b. Across the entire range,

the amphiboles show very similar trace element partitioning trends, but absolute $D^{Amph/L}$ values differ by up to an order of magnitude. The KMB host melt amphiboles crystallized at slightly lower temperatures and pressures (Merrill and Wyllie, 1975) than the majority of experimental studies in the literature.

High charge (>3+) trace element partitioning in titanium-rich amphibole has strong inverse correlation with Mg#. D_{Nb} and D_{Ta} are strongly affected by Mg# (Tiepolo et al., 2000b, 2001), but also show moderate correlation with TiO_2 content in the amphibole. The K1amphA Nb and Ta partition coefficients agree well with these previous results. D_{Nb}/D_{Ta} increases with decreasing Mg#, becoming greater than unity for Mg# $< \sim$63 (Tiepolo et al., 2000b, 2001). The K1amphA D_{Nb}/D_{Ta} plots just below the general trend, which suggests that the cooler formation conditions of the KMB host melt amphibole may have an effect on the ratio. From these same studies, D_{Zr} and D_{Hf} exhibit moderate inverse correlation to Mg# but D_{Zr}/D_{Hf} changes little for the entire range of (titanian pargasite–kaersutite) amphibole compositions and is always less than unity. K1amphA D_{Zr} and D_{Hf} are in agreement with previous experimental results. D_{Nb}/D_{Zr} has strong inverse correlation to Mg# and K1amphA fits well with the literature trend. Uranium and Th are both highly incompatible in amphibole; the presence of U^{5+} and U^{6+} does not seem to have a large effect on amphibole–melt partitioning of uranium, in contrast with garnet.

Tungsten partitioning is poorly studied due to the difficulties in measuring low W concentrations in most silicates. Tungsten concentrations in amphibole are typically very low, but variation is apparent as KMB amphibole megacrysts have up to 5.5 times lower W concentrations than the KMB host melt amphibole (K1amphA). D_W for K1amphA is 0.075, which is significantly larger than that observed by Adam and Green (2006) ($D_W = 0.0011$–0.0025, Mg# $= \sim$0.79). K1amphA has a lower Mg#, so it is unclear if the partitioning difference is due to formation conditions or amphibole composition. D_{Hf}/D_W for K1amphA is 6.1, which is significantly smaller than Adam and Green (2006) ($D_{Hf}/D_W \sim$240). Taken at face value, this suggests Mg-rich amphiboles formed at greater depth apparently are able to fractionate Hf from W to a larger extent, but more work is needed to test this hypothesis.

The K1amphA REE partition coefficients are in general agreement with previous studies. The maximum D_{REE} in K1amphA occurs for Gd, which is a lower mass REE than reported elsewhere including Dy (Tiepolo et al., 2000a) and Ho (Dalpé and Baker, 2000). The KMB D_{LILE} values are slightly higher than observed in experiments but deviate much less than observed with the KMB garnet megacrysts.

5. DISCUSSION

5.1. KMB mineral formation conditions

In order to properly compare partition coefficients from natural systems to experiments, the mineral formation conditions must be carefully assessed. Merrill and Wyllie (1975) used petrographic analysis of KMB samples in conjunction with high-temperature–high-pressure experiments to infer formation conditions of the KMB megacrysts. The authors concluded that the large garnet, clinopyroxene, and amphibole megacrysts could crystallize simultaneously from a H_2O-rich nephelinitic melt at pressures between 2.2 and 2.4 GPa and temperatures between 1100 and 1200 °C. Clinopyroxene-garnet Fe/Mg exchange geothermometry (Ravna, 2000b) can also be applied to the co-crystallizing KMB megacrystic phases to calculate formation conditions. Clast 5 of this study is coarse and bimineralic, composed of garnet K5grt and clinopyroxene K5cpx (Table 1). For an assumed pressure of 2.2 GPa that is the minimum pressure necessary for garnet crystallization in a hydrous nephelinite melt (Merrill and Wyllie, 1975), the bimineralic garnet-clinopyroxene megacryst yields a formation temperature of 1105 °C. The KMB megacrysts of Dickey (1968) yield a similar formation temperature of 1076 °C. The Ravna (2000b) Fe/Mg geothermometer requires an Fe^{3+} correction. Ferric iron to total iron percentages for the garnet ($Fe^{3+}/Fe^{T} \sim$10%), clinopyroxene (~35%), and amphibole (~30%) were estimated based on previous results of KMB megacrysts determined from wet chemistry methods (Dickey, 1968; Mason, 1968), Mössbauer spectroscopy (Dyar et al., 1993), and stoichiometry estimations (White et al., 1972; Zack et al., 1997). We feel that these high Fe^{3+}/Fe^{T} percentages are reasonable given that the KMB nephelinite host melt was fluid-rich, resulting in highly oxidizing conditions and only minor observed Eu anomalies.

Zack et al. (1997) calculated formation temperatures for coexisting garnet and clinopyroxene phases in seven polycrystalline KMB amph-grt-cpx nodules of 920 ± 30 °C at an assumed pressure of 1.5 GPa. Recalculation of the temperature using a pressure of 2.2 GPa yields 960 °C, which is still significantly lower than observed for the KMB megacryst phases. Merrill and Wyllie (1975) suggest that subsolidus re-equilibration of the polycrystalline amph-grt-cpx nodules could occur at 800 °C and 2–3 GPa. Re-equilibration would account for the clinopyroxene exsolution textures observed in these nodules and decrease the calculated formation temperature due to Fe–Mg exchange in the cpx phase.

The hornblende-garnet Fe/Mg exchange geothermometer (Ravna, 2000a) allows for a second formation temperature estimate. However, application of the geothermometer to the KMB amphibole and garnet megacrysts yields unrealistic temperatures exceeding 3000 °C. From these results, Fe–Mg exchange between the amphibole and the garnet megacrysts could not have occurred. Since the amphibole megacrysts have significantly lower initial Hf isotope compositions than the other phases analyzed in this study, these results suggest that the amphibole megacrysts formed independently in unrelated conditions. Finally, Merrill and Wyllie (1975) propose that the host melt amphibole (K1amphA) was among the latest-forming mineral phases of the nephelinite melt system and likely crystallized from the ascending magma at pressures between 1.3 and 2.4 GPa.

5.2. Mineral–melt partitioning

Logarithmic partition coefficients $\log(D_i)$ for trace elements i were first observed to show near-parabolic depen-

dence on the trace element ionic radius r_i by Onuma et al. (1968). The empirical observation that the maximum partition coefficient in such so-called Onuma diagrams often occurs at radii that are close to the radius of the crystallographic site on which elements i partition ultimately led to the development of the so-called crystal lattice-strain partitioning model (Blundy and Wood, 1994). This model assumes that the energetics of trace element substitution into a crystallographic site are dominated by the crystal lattice-strain energy required to accommodate misfit. The resulting lattice-strain model (Eq. (1)) includes three parameters to describe mineral/melt partitioning ($D^{Min/L}$): (1) the 'ideal radius' r_0 for a given element with charge j+ that does not strain the crystal lattice and therefore allows for maximum trace element incorporation, (2) the maximum partition coefficient D_0 for this 'ideal radius' element, and (3) the apparent Young's modulus E of the site, which relates the resistance to trace element incorporation to the local elasticity of the crystal lattice.

$$D_i = D(r_i) = D_0 \exp\left(\frac{-4\pi E N_A}{RT}\left(\frac{r_0}{2}(r_i - r_0)^2 - \frac{1}{3}(r_i - r_0)^3\right)\right) \quad (1)$$

where R is the universal gas constant, T is the temperature in Kelvin, and N_A is Avogadro's Number.

Aluminosilicate garnets ($X_3^{VIII}Al_2^{VI}Si_3^{IV}O_{12}$, where X = Ca^{2+}, Mg^{2+}, Fe^{2+}, or Mn^{2+} and Roman numerals denote coordination numbers) can incorporate a wide range of trace elements into their structure. The REE series (including Y and Sc as they are chemically very similar) is known to substitute almost exclusively with the major divalent cations in the large dodecahedral garnet X site (Quartieri et al., 1999, 2004). The derived $D^{Grt/L}$ values from the ICP-MS data set are plotted in Onuma diagrams are plotted as a function of ionic radius in Fig. 7a. The trivalent cation partition coefficients for the garnet megacrysts are extremely well described by the crystal lattice-strain model for ions with radii smaller than ~1.1 Å. A least-squared best fit of the HREE, MREE, and Sc partition coefficients yields $r_0 = 0.936 \pm 0.002$ Å, $D_0 = 10.5 \pm 0.4$, and $E = 557 \pm 28$ GPa for $T = 1105$ °C (Fig. 7a), in excellent agreement with crystal lattice-strain model expectations. The only partition coefficients that do not fall directly on the best fit curve are the LREE, in agreement with the earlier observations that La and Ce concentrations in KMB garnet are enriched relative to the general REE trend. As discussed in the previous section for LILE, sub-micron fluid inclusions rich in LREE could be a possible cause for the enrichment. The very low concentrations of La and Ce in garnet ($\ll$1 ppm) make these elements most susceptible to enrichment. If fluid inclusions are the cause, the deviation of D_{La} from the Onuma parabolic trend can be explained by the presence of only ~350 ppb La more than expected. Since La has the highest fluid solubility of the REE, this places an upper limit for the amount of LREE that would be present in the fluid inclusions. The heavier REE concentrations in the fluid inclusions would be significantly lower due to decreased solubility. Alternatively, loss of a volatile-rich phase during eruption could result in selective removal of a proportion of the fluid-mobile elements from the ascending melt. However, this mechanism would have the strongest effect only on the most fluid-soluble elements, including LILE and to a lesser extent the LREE.

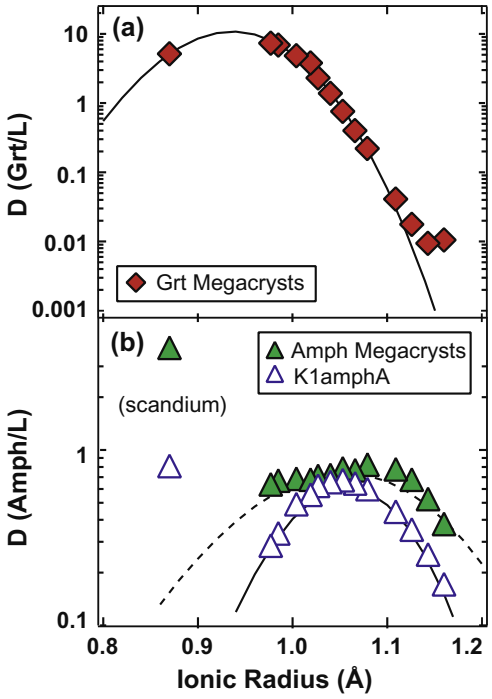

Fig. 7. KMB mineral–melt REE partition coefficients plotted vs. ionic radii (Shannon, 1976) for (a) garnet and (b) amphibole with fits using the crystal lattice-strain partitioning model (Eq. (1); see also Blundy and Wood, 1994). For the garnet, only the MREE, HREE, and Sc were used in the modeling as the LREE show anomalous enrichment, potentially due to sub-micron fluid inclusions (see also Fig. 4). The host melt amphibole (K1amphA) has significantly different partition coefficients from the amphibole megacrysts. The partition coefficients for K1amphA agree very well with crystal lattice-strain model expectations, whereas the amphibole megacryst data show significantly more scatter. In addition, the amphibole megacrysts have an unreasonably small apparent Young's Modulus (E, see Eq. (1)), resulting in an unrealistically broad parabolic trend. Scandium is excluded from the amphibole modeling as it appears to occupy a different structural site.

Some attempts have been made to generalize garnet REE trace element partitioning variations as a function of pressure, temperature, and garnet and melt composition in garnet by means of thermodynamic or statistical modeling (Draper and van Westrenen, 2007; van Westrenen and Draper, 2007). Their predictive equations yield values of 0.914 Å for r_0 and 626 GPa for E, assuming $P = 2.2$ GPa and $T = 1105$ °C as obtained from thermobarometry (Section 5.1), in reasonable agreement with observations. The statistical formulation for D_0 (Draper and van Westrenen, 2007) yields a value of 4.2, giving the correct order of magnitude but underestimating the parabola amplitude by a factor of 2.5. The thermodynamic model (van Westrenen and Draper, 2007) is not applicable to low T, hydrous-rich melt systems such as the KMB [or the deep subduction zone melts investigated by Klimm et al. (2008)] as the formulation is only rigorous for anhydrous melt systems. The

resulting D_0 from the thermodynamic model is several orders of magnitude larger than what we observe, showing the important controls that volatiles can exert on partition coefficients in hydrous melt systems.

The use of Onuma diagrams with tetravalent cations in garnet would be highly desirable, but a number of problems hinder the procedure (van Westrenen et al., 2001a; Dwarzski et al., 2006). Titanium, Zr and Hf are believed to preferentially enter the octahedral Y site of garnet by replacing Al, but Zr and Hf have very similar ionic radii that are close to the expected r_0 value for the octahedral Y site, resulting in poorer lattice constraints than are possible with REE partitioning into the X site. The $HFSE^{4+}$, U^{4+} and Th^{4+} may also partition into the X site for high CaO garnets (19–40% grossular) (van Westrenen et al., 2001a), although D_U may also be affected by fO_2 and should only be used for fitting in low fO_2 systems. Thus, tetravalent partition coefficient sets are less well-constrained and can only be fit by the asymmetric parabolic curves of the crystal lattice-strain theory with additional assumptions (van Westrenen et al., 2001a). These problems are even more severe for the pentavalent ions since only Nb and Ta can substitute into a lattice site and each have nearly identical ionic radii.

Amphibole crystal structure allows for considerably more compositional variation than is observed in garnet due to the presence of five separate sites for cation occupation. In situ compositional analysis and partitioning studies of titanian pargasite demonstrate that the trivalent REE and Y partition into the $M4^{VIII}$ site (Dalpé and Baker, 2000; Tiepolo et al., 2001; references therein). The derived $D^{Amph/L}$ values for both K1amphA and the average KMB amphibole megacrysts are plotted in Fig. 7b as a function of ionic radii. The K1amphA partition coefficients have a much smoother pattern than the amphibole megacrysts and conform better to Eq. (1). The best fit parameters from the crystal lattice-strain theory for K1amphA yields $r_0 = 1.058 \pm 0.001$ Å, $D_0 = 0.61 \pm 0.01$, and $E = 334 \pm 13$ GPa for $T = 1000$ °C, in agreement with amphibole crystal lattice expectations. Scandium is excluded from the amphibole fitting as it appears to occupy a different structural site. The limited number of different ionic radii for tetravalent or pentavalent ions precludes the construction of Onuma diagrams and the determination of site-specific parameters for amphibole.

The amphibole megacrysts have consistently higher calculated partition coefficients and a significantly more irregular partitioning pattern than the host melt amphibole (Fig. 7b). Onuma diagram analyses therefore confirm the Hf isotope disequilibrium of the amphibole megacrysts with the other phases, showing (a) that the garnet megacrysts and host melt amphibole were formed in equilibrium with the nephelinite melt and (b) in contrast, the amphibole megacrysts cannot have grown in full chemical equilibrium with the nephelinite host melt.

5.3. Assessment of mineral–melt equilibrium

Overall, our data provide four independent lines of evidence that support the hypothesis that the KMB garnet megacryst, host melt amphibole, and nephelinite host melt attained mineral–melt equilibrium with each other. First, the KMB megacrysts do not exhibit any solid-state deformation or exsolution textures, and all garnets and amphiboles are not zoned and have highly uniform compositions across the entire hand specimen. These results are not surprising as the Kakanui megacrysts are renowned for their compositional uniformity in both major and trace elements. The widespread use of KMB megacrystic garnet and augite as electron microprobe standards has shown no obvious evidence for sample inhomogeneity (e.g., Czamanske et al., 1993; Günther et al., 1997; Jarosewich, 2002).

Second, the Lu–Hf isotope systematics for the garnet megacrysts, host melt amphibole, and nephelinite host melt (Fig. 3) define an isochron in a Lu–Hf isotope evolution relationship with a slope consistent with the previously published apparent eruption age for the KMB of ~34 Ma (Hoernle et al., 2006). Since elemental equilibrium is a pre-requisite for isotope equilibrium, the Lu–Hf isotope data are consistent with full elemental equilibrium among these phases. Additionally, the highly uniform amphibole megacrysts have a distinct Hf isotopic composition that significantly differs from all other phases investigated in this study. The initial $\varepsilon_{Hf}(t)$ value of the amphibole megacrysts for $T = 34.1$ Ma is approximately 2.5 ε_{Hf} units lower than the other measured values, precluding it from being in isotopic equilibrium with the other mineral phases and the host melt. Similar deviations were observed by Hoernle et al. (2006) for other Kakanui amphibole megacrysts using Sr–Nd–Pb isotope systematics. The use of Sr and Pb isotopes to test equilibrium may be biased in altered or metasomaticly overprinted rock suites because these elements are considered fluid-mobile with low closure temperatures in most mineral phases. Hence, Hf isotope systematics may be a more robust and reliable test of equilibrium in future studies due to the immobile nature of Hf in fluids.

Third, the systematics of the mineral/melt partition coefficients for the garnet megacrysts and host melt amphibole (Fig. 7) provide further support for mineral–melt equilibrium. The partition coefficients for fluid-immobile elements, including heavy and middle REE, are well described by the crystal lattice-strain model and yield lattice parameters in excellent agreement with model expectations. Such excellent fits are not possible if the mineral phases and host melt do not share a common genetic origin and maintain chemical equilibrium from formation to eruption. This is illustrated by our Onuma diagram analysis of the amphibole megacryst–melt REE partition coefficients, which are not described well by the crystal lattice-strain model: the predicted Young's modulus for the amphibole megacrysts is significantly smaller than previously reported values (Dalpé and Baker, 2000), resulting in an unreasonable lattice structure for poorly discriminating trace element accommodation (Fig. 7b).

Finally, Fe–Mg exchange thermometry of coexisting KMB garnet and clinopyroxene megacrysts from bimineralic grt-cpx coarse aggregates yields formation temperature estimates that agree with the high P–T experimental studies of Merrill and Wyllie (1975), who studied these same Kakanui rocks. The amphibole megacrysts never form

coarse aggregates with garnet or clinopyroxene megacrysts in the KMB, and Fe–Mg exchange thermometry of megacrystic garnet and hornblende yields unreasonably high temperature estimates of >3000 °C. The amphibole megacrysts therefore could not have been in Fe–Mg exchange with the garnet (and clinopyroxene) megacrysts, while the garnet and clinopyroxene megacrysts crystallized in the same conditions and retained their major element equilibrium following eruption.

From these independent lines of evidence, we conclude that the KMB garnet megacrysts, host melt amphibole and nephelinite are in chemical equilibrium with each other. Therefore, the partition coefficients for the immobile elements including the MREE, HREE and HFSE must be valid, allowing a comparison of partition coefficients from this natural system to the results from high *P–T* experimental studies. Conversely, the amphibole megacrysts cannot have formed in equilibrium with the KMB nephelinite and thus should not be used to determine partition coefficients. The presence of these "xenocrystic" amphibole crystals stresses the importance of establishing mineral–melt equilibrium when studying natural systems.

5.4. Implications for HFSE fractionation in magmatic systems

Our new data set shows that $HFSE^{5+}$ are highly incompatible in garnet. The overall low abundance of these elements in garnet renders this mineral less important in mass balancing Nb and Ta in magmatic systems than previously thought. In addition, both Nb and Ta have nearly identical ionic radii and show very similar partitioning behavior in the KMB garnets, implying no significant fractionation of Nb from Ta with residual garnet. Previously reported orders of magnitude differences between Nb and Ta partitioning in garnet are not supported by our results (Zack et al., 1997; Green et al., 2000), and may be due to difficulties in analyses of these elements. Compared to garnet, amphibole contains much higher concentrations of Nb and Ta, and is thus of greater importance for the Nb–Ta budget of hydrous igneous systems. Because many island arc rocks show amphibole cumulates in deep rooted magma chambers in evolved evolutionary stages, some of the observed Nb–Ta depletion in island arc rocks could be accounted for with residual amphibole. However, the narrow stability field of amphiboles renders the role of residual amphiboles less important compared to rutile or other accessory phases that contain high HFSE contents. Most importantly, the Nb/Ta in the amphiboles analyzed here are sub-chondritic, in agreement with most observed terrestrial rocks. Thus residual amphiboles with Mg# > 55, including the majority of mantle-derived amphiboles, do not constitute a high Nb/Ta reservoir (Tiepolo et al., 2000b).

Concerning Zr/Hf, amphibole fractionation can cause super-chondritic Zr/Hf in a coexisting melt, whereas garnet fractionation will have the opposite effect. Accordingly, partial melting in the garnet stability field can result in a derived melt with sub-chondritic Zr/Hf. In addition to the widely accepted hypothesis that elevated Zr/Hf in ocean island basalt are caused by residual clinopyroxene (Pfänder et al., 2007b), garnet may act in an opposite manner to lower Zr/Hf for melts originating in the garnet stability field depending on melt fraction.

Our W partition coefficients further show that garnet cumulate crystallization can cause moderate to strong Hf–W and Nb–Zr fractionation in magmatic systems. This can be of particular importance with respect to the distribution of live ^{182}Hf and ^{92}Nb in the Hadean Eon. Large scale garnet crystallization in a magma ocean may have caused an early radiogenic ^{182}W reservoir compared to the ambient mantle and the non-radiogenic core. For Zr–Nb, the opposite effect would have been the case with non-radiogenic $^{92}Zr/^{90}Zr$ in the garnet cumulates and radiogenic signatures in the residual melt. Despite the high Zr concentrations of ~70 ppm in the garnet, this effect would not be strong due to a low initial ^{92}Nb abundance (Schönbächler et al., 2003, 2005), but may prove important in future studies exploring early Earth dynamics.

More importantly, however, is the incompatible nature of HFSE in the analyzed silicate phases, which has partly led to the significant concentration of HFSE into crustal rocks. As this is one of the first studies in which Zr, Hf, Nb, Ta, and W partition coefficients have been measured on the same sample, our consistent dataset show that garnet and amphibole may result in characteristic trace element signatures in residual melts. This may be useful for developing characteristic HFSE isotopic fingerprinting that would be indicative of the mineral phases studied here.

6. CONCLUSIONS

We demonstrate that the isotope dilution technique for analyzing HFSE in natural samples can be used to obtain high-precision mineral–melt partition coefficient data. Natural phenocryst–host melt systems can be used to derive partition coefficients, providing a complementary and independent check on the results of high-pressure experiments, which use less precise HFSE analytical techniques. We have shown that a combination of isotopic measurements, major/trace element partitioning data, and petrographic analysis provides excellent tools to test equilibrium between minerals and melt in natural magmatic systems. In particular, Hf isotope compositions are shown to be a powerful tool to test mineral phase–host melt equilibrium and we suggest the use of this tool in future *D* value determinations using natural samples. This is particularly true in light of possible LREE (Nd) and LILE (Rb, Pb) disturbance in natural systems due to element mobility that could affect Sm–Nd, Rb–Sr, or U–Pb isotope ratios but leave Lu–Hf effectively pristine.

Our new dataset suggests that garnet plays a much less significant role in fractionating Nb–Ta in magmatic systems than previously thought. Amphibole may be of greater importance but its narrow *P–T* stability field limits its influence. Accordingly, other (accessory) phases such as zircon, allanite or rutile are most likely of much higher significance for HFSE, as suggested previously (Rubatto and Hermann, 2007; Klimm et al., 2008; Hermann and Rubatto, 2009; Schmidt et al., 2009).

ACKNOWLEDGMENTS

Yona Nebel-Jacobsen, Carsten Münker, and Peter Sprung are thanked for field assistance. E.C.F. acknowledges funding from the Huygens Scholarship Programme (Netherlands Ministry of Education, Culture and Science). W.v.W. thanks the European Science Foundation for financial support. The MC-ICP-MS facility was supported by a grant (175.107.404.01) from the Netherlands Organisation for Scientific Research (NWO/ALW). Bas van der Wagt and Richard Smeets are kindly acknowledged for ICP-MS and laboratory assistance, and Wim Lustenhouwer is kindly thanked for electron microprobe support. Alexander Schmidt, two anonymous reviewers, and Associate Editor Frederick Frey are thanked for constructive comments that led to the improvement of this manuscript.

REFERENCES

Adam J. and Green T. (2006) Trace element partitioning between mica- and amphibole-bearing garnet lherzolite and hydrous basanitic melt: 1. Experimental results and the investigation of controls on partitioning behaviour. *Contrib. Mineral. Petrol.* **152**, 1–17.

Adam J., Green T. H. and Sie S. H. (1993) Proton microprobe determined partitioning of Rb, Sr, Ba, Y, Zr, Nb and Ta between experimentally produced amphiboles and silicate melts with variable F content. *Chem. Geol.* **109**, 29–49.

Adam J., Oberti R., Cámara F. and Green T. H. (2007) An electron microprobe, LAM-ICP-MS and single-crystal X-ray structure refinement study of the effects of pressure, melt-H_2O concentration and fO_2 on experimentally produced basaltic amphiboles. *Eur. J. Mineral.* **19**, 641–655.

Amelin Y., Lee D. C., Halliday A. N. and Pidgeon R. T. (1999) Nature of the Earth's earliest crust from hafnium isotopes in single detrital zircons. *Nature* **399**, 252–255.

Barth M. G., Foley S. F. and Horn I. (2002) Partial melting in Archean subduction zones: constraints from experimentally determined trace element partition coefficients between eclogitic minerals and tonalitic melts under upper mantle conditions. *Precambrian Res.* **113**, 323–340.

Barth M. G., McDonough W. F. and Rudnick R. L. (2000) Tracking the budget of Nb and Ta in the continental crust. *Chem. Geol.* **165**, 197–213.

Beattie P. (1993) Uranium thorium disequilibria and partitioning on melting of garnet peridotite. *Nature* **363**, 63–65.

Bizzarro M., Baker J. A., Haack H., Ulfbeck D. and Rosing M. (2003) Early history of Earth's crust–mantle system inferred from hafnium isotopes in chondrites. *Nature* **421**, 931–933.

Blichert-Toft J. and Albarède F. (1997) The Lu–Hf isotope geochemistry of chondrites and the evolution of the mantle–crust system. *Earth Planet. Sci. Lett.* **148**, 243–258.

Blichert-Toft J., Chauvel C. and Albarède F. (1997) Separation of Hf and Lu for high-precision isotope analysis of rock samples by magnetic sector-multiple collector ICP-MS. *Contrib. Mineral. Petrol.* **127**, 248–260.

Blundy J. and Wood B. (1994) Prediction of crystal-melt partition-coefficients from elastic-moduli. *Nature* **372**, 452–454.

Bouvier A., Vervoort J. D. and Patchett P. J. (2008) The Lu–Hf and Sm–Nd isotopic composition of CHUR: constraints from unequilibrated chondrites and implications for the bulk composition of terrestrial planets. *Earth Planet. Sci. Lett.* **273**, 48–57.

Brenan J. M., Shaw H. F., Phinney D. L. and Ryerson F. J. (1994) Rutile-aqueous fluid partitioning of Nb, Ta, Hf, Zr, U and Th – implications for high-field strength element depletions in island-arc basalts. *Earth Planet. Sci. Lett.* **128**, 327–339.

Brenan J. M., Shaw H. F., Ryerson F. J. and Phinney D. L. (1995) Experimental-determination of trace-element partitioning between pargasite and a synthetic hydrous Andesitic melt. *Earth Planet. Sci. Lett.* **135**, 1–11.

Chauvel C. and Blichert-Toft J. (2001) A hafnium isotope and trace element perspective on melting of the depleted mantle. *Earth Planet. Sci. Lett.* **190**, 137–151.

Chauvel C., Lewin E., Carpentier M., Arndt N. T. and Marini J. C. (2008) Role of recycled oceanic basalt and sediment in generating the Hf–Nd mantle array. *Nat. Geosci.* **1**, 64–67.

Chauvel C., Marini J. C., Plank T. and Ludden J. N. (2009) Hf–Nd input flux in the Izu-Mariana subduction zone and recycling of subducted material in the mantle. *Geochem. Geophys. Geosyst.* **10**, Q01001.

Corcoran P. L. and Moore L. N. (2008) Subaqueous eruption and shallow-water reworking of a small-volume Surtseyan edifice at Kakanui, New Zealand. *Can. J. Earth Sci.* **45**, 1469–1485.

Czamanske G. K., Sisson T. W., Campbell J. L. and Teesdale W. J. (1993) Micro-PIXE analysis of silicate reference standards. *Am. Mineral.* **78**, 893–903.

Dalpé C. and Baker D. R. (2000) Experimental investigation of large-ion-lithophile-element-, high-field-strength-element- and rare-earth-element-partitioning between calcic amphibole and basaltic melt: the effects of pressure and oxygen fugacity. *Contrib. Mineral. Petrol.* **140**, 233–250.

David K., Schiano P. and Allègre C. J. (2000) Assessment of the Zr/Hf fractionation in oceanic basalts and continental materials during petrogenetic processes. *Earth Planet. Sci. Lett.* **178**, 285–301.

Dickey J. S. (1968) Eclogitic and other inclusions in the mineral Breccia member of Deborah Volcanic formation at Kakanui New Zealand. *Am. Mineral.* **53**, 1304–1319.

Draper D. S. and van Westrenen W. (2007) Quantifying garnet–melt trace element partitioning using lattice-strain theory: assessment of statistically significant controls and a new predictive model. *Contrib. Mineral. Petrol.* **154**, 731–746.

Dwarzski R. E., Draper D. S., Shearer C. K. and Agee C. B. (2006) Experimental insights on crystal chemistry of high-Ti garnets from garnet–melt partitioning of rare-earth and high-field-strength elements. *Am. Mineral.* **91**, 1536–1546.

Dyar M. D., Mackwell S. J., Mcguire A. V., Cross L. R. and Robertson J. D. (1993) Crystal-chemistry of Fe^{3+} and H^+ in mantle Kaersutite – implications for mantle metasomatism. *Am. Mineral.* **78**, 968–979.

Foley S. F., Barth M. G. and Jenner G. A. (2000) Rutile/melt partition coefficients for trace elements and an assessment of the influence of rutile on the trace element characteristics of subduction zone magmas. *Geochim. Cosmochim. Acta* **64**, 933–938.

Gage M. (1965) The geology of the Waitaki subdivision. *NZ Geol. Surv. Bull. (n.s.)* **55**, 1–135.

Green T. H. and Adam J. (2003) Experimentally-determined trace element characteristics of aqueous fluid from partially dehydrated mafic oceanic crust at 3.0 GPa, 650–700 degrees C. *Eur. J. Mineral.* **15**, 815–830.

Green T. H., Blundy J. D., Adam J. and Yaxley G. M. (2000) SIMS determination of trace element partition coefficients between garnet, clinopyroxene and hydrous basaltic liquids at 2–7.5 GPa and 1080–1200 degrees C. *Lithos* **53**, 165–187.

Günther D., Frischknecht R., Heinrich C. A. and Kahlert H. J. (1997) Capabilities of an argon fluoride 193 nm excimer laser for laser ablation inductively coupled plasma mass spectometry microanalysis of geological materials. *J. Anal. Atom. Spectrom.* **12**, 939–944.

Harper C. L. (1996) Evidence for ^{92g}Nb in the Early Solar System and Evaluation of a new p-process cosmochronometer from ^{92g}Nb/^{92}Mo. *Astrophys. J.* **466**, 437–456.

Harrison T. M., Blichert-Toft J., Muller W., McCulloch M., Albarède F., Mojzsis S. J. and Holden P. (2005) Heterogeneous Hadean hafnium: evidence of continental crust by 4.5 Ga? *Geochim. Cosmochim. Acta* **69**, A390.

Hauri E. H., Wagner T. P. and Grove T. L. (1994) Experimental and natural partitioning of Th, U, Pb and other trace-elements between garnet, clinopyroxene and basaltic melts. *Chem. Geol.* **117**, 149–166.

Hermann J. and Rubatto D. (2009) Accessory phase control on the trace element signature of sediment melts in subduction zones. *Chem. Geol.* **265**, 512–526.

Hoernle K., White J. D. L., van den Bogaard P., Hauff F., Coombs D. S., Werner R., Timm C., Garbe-Schonberg D., Reay A. and Cooper A. F. (2006) Cenozoic intraplate volcanism on New Zealand: upwelling induced by lithospheric removal. *Earth Planet. Sci. Lett.* **248**, 350–367.

Ionov D. A. and Hofmann A. W. (1995) Nb–Ta-rich mantle amphiboles and micas – implications for subduction-related metasomatic trace-element fractionations. *Earth Planet. Sci. Lett.* **131**, 341–356.

Irving A. J. and Frey F. A. (1978) Distribution of trace-elements between garnet megacrysts and host volcanic liquids of kimberlitic to rhyolitic composition. *Geochim. Cosmochim. Acta* **42**, 771–787.

Irving A. J. and Frey F. A. (1984) Trace-element abundances in megacrysts and their host basalts – constraints on partition-coefficients and megacryst genesis. *Geochim. Cosmochim. Acta* **48**, 1201–1221.

Jarosewich E. (2002) Smithsonian microbeam standards. *J. Res. Natl. Inst. Stand. Technol.* **107**, 681–685.

Johnson K. T. M. (1998) Experimental determination of partition coefficients for rare earth and high-field-strength elements between clinopyroxene, garnet, and basaltic melt at high pressures. *Contrib. Mineral. Petrol.* **133**, 60–68.

Kamber B. S. and Collerson K. D. (2000) Role of 'hidden' deeply subducted slabs in mantle depletion. *Chem. Geol.* **166**, 241–254.

Kleine T., Münker C., Mezger K. and Palme H. (2002) Rapid accretion and early core formation on asteroids and the terrestrial planets from Hf–W chronometry. *Nature* **418**, 952–955.

Klemme S., Blundy J. D. and Wood B. J. (2002) Experimental constraints on major and trace element partitioning during partial melting of eclogite. *Geochim. Cosmochim. Acta* **66**, 3109–3123.

Klimm K., Blundy J. D. and Green T. H. (2008) Trace element partitioning and accessory phase saturation during H_2O-saturated melting of basalt with implications for subduction zone chemical fluxes. *J. Petrol.* **49**, 523–553.

König S., Münker C., Schuth S. and Garbe-Schönberg D. (2008) Mobility of tungsten in subduction zones. *Earth Planet. Sci. Lett.* **274**, 82–92.

LaTourrette T., Hervig R. L. and Holloway J. R. (1995) Trace-element partitioning between amphibole, phlogopite, and basanite melt. *Earth Planet. Sci. Lett.* **135**, 13–30.

Leake B. E., Woolley A. R., Arps C. E. S., Birch W. D., Gilbert M. C., Grice J. D., Hawthorne F. C., Kato A., Kisch H. J., Krivovichev V. G., Linthout K., Laird J., Mandarino J. A., Maresch W. V., Nickel E. H., Rock N. M. S., Schumacher J. C., Smith D. C., Stephenson N. C. N., Ungaretti L., Whittaker E. J. W. and Guo Y. Z. (1997) Nomenclature of amphiboles: report of the subcommittee on amphiboles of the International Mineralogical Association, commission on new minerals and mineral names. *Am. Mineral.* **82**, 1019–1037.

Ludwig K. R. (2001) Isoplot/Ex version 2.49; a geochronological toolkit for Mocrosoft Excel. *Berkeley Geochronol. Center Spec. Publ.* **1A.**

Mason B. (1968) Eclogitic Xenoliths from Volcanic Breccia at Kakanui, New Zealand. *Contrib. Mineral. Petrol.* **19**, 316–327.

Mason B. and Allen R. O. (1973) Minor and trace-elements in augite, hornblende, and pyrope megacrysts from Kakanui, New-Zealand. *NZ J. Geol. Geop.* **16**, 935–947.

McDonough W. F. (1991) Partial melting of subducted oceanic crust and isolation of its residual eclogitic lithology. *Phil. Trans. R. Soc. Lond. A* **335**, 407–418.

McDonough W. F. and Sun S. S. (1995) The composition of the earth. *Chem. Geol.* **120**, 223–253.

Merrill R. B. and Wyllie P. J. (1975) Kaersutite and Kaersutite Eclogite from Kakanui, New Zealand – Water-excess and water-deficient melting to 30 kilobars. *Geol. Soc. Am. Bull.* **86**, 555–570.

Morel M. L. A., Nebel O., Nebel-Jacobsen Y. J., Miller J. S. and Vroon P. Z. (2008) Hafnium isotope characterization of the GJ-1 zircon reference material by solution and laser-ablation MC-ICPMS. *Chem. Geol.* **255**, 231–235.

Münker C., Pfänder J. A., Weyer S., Büchl A., Kleine T. and Mezger K. (2003) Evolution of planetary cores and the earth–moon system from Nb/Ta systematics. *Science* **301**, 84–87.

Münker C., Weyer S., Mezger K., Rehkämper M., Wombacher F. and Bischoff A. (2000) ^{92}Nb-^{92}Zr and the early differentiation history of planetary bodies. *Science* **289**, 1538–1542.

Münker C., Weyer S., Scherer E. and Mezger K. (2001) Separation of high field strength elements (Nb, Ta, Zr, Hf) and Lu from rock samples for MC-ICPMS measurements. *Geochem. Geophys. Geosyst.* **2**, 1064.

Münker C., Wörner G., Yogodzinski G. and Churikova T. (2004) Behaviour of high field strength elements in subduction zones: constraints from Kamchatka-Aleutian arc lavas. *Earth Planet. Sci. Lett.* **224**, 275–293.

Nebel O., Morel M. L. A. and Vroon P. Z. (2009) Isotope dilution analyses of Lu, Hf, Zr, Ta, and W, and Hf-isotope compositions of NIST SRM 610 and SRM-612 glass wafers. *Geostand. Geoanal. Res.* **33**, 487–499.

Nebel O., Münker C., Nebel-Jacobsen Y. J., Kleine T., Mezger K. and Mortimer N. (2007a) Hf–Nd–Pb isotope evidence from Permian arc rocks for the long-term presence of the Indian-Pacific mantle boundary in the SW Pacific. *Earth Planet. Sci. Lett.* **254**, 377–392.

Nebel O., Nebel-Jacobsen Y., Mezger K. and Berndt J. (2007b) Initial Hf isotope compositions in magmatic zircon from early Proterozoic rocks from the Gawler Craton, Australia: a test for zircon model ages. *Chem. Geol.* **241**, 23–37.

Nebel O., Vroon P. Z., de Vries D. F. W., Jenner F. E. and Mavrogenes J. A. (2010) Tungsten isotopes as tracers of core–mantle interactions: the influence of subducted sediments. *Geochim. Cosmochim. Acta* **74**, 751–762.

Nelson C. S., Lee D., Maxwell P., Maas R., Kamp P. J. J. and Cooke S. (2004) Strontium isotope dating of the New Zealand Oligocene. *NZ J. Geol. Geophys.* **47**, 719–730.

Onuma N., Higuchi H., Wakita H. and Nagasawa H. (1968) Trace element partition between two pyroxenes and host lava. *Earth Planet. Sci. Lett.* **5**, 47–51.

Patchett P. J. (1983) Hafnium isotope results from mid-ocean ridges and kerguelen. *Lithos* **16**, 47–51.

Patchett P. J., Kouvo O., Hedge C. E. and Tatsumoto M. (1981) Evolution of continental crust and mantle heterogeneity: evidence from Hf isotopes. *Contrib. Mineral. Petrol.* **78**, 279–297.

Pearce J. A., Kempton P. D., Nowell G. M. and Noble S. R. (1999) Hf–Nd element and isotope perspective on the nature and

provenance of mantle and subduction components in Western Pacific arc-basin systems. *J. Petrol.* **40**, 1579–1611.

Pertermann M., Hirschmann M. M., Hametner K., Günther D. and Schmidt M. W. (2004) Experimental determination of trace element partitioning between garnet and silica-rich liquid during anhydrous partial melting of MORB-like eclogite. *Geochem. Geophys. Geosyst.* **5**, Q05A01.

Pfänder J. A., Jung S., Münker C. and Mezger K. (2007a) High-field strength elements (Nb, Ta, Zr, Hf) in continental basalts from the CEVP – implications for the HFSE budget of the lithospheric mantle and the global Nb budget. *Geochim. Cosmochim. Acta* **71**, A784.

Pfänder J. A., Münker C., Stracke A. and Mezger K. (2007b) Nb/Ta and Zr/Hf in ocean island basalts – implications for crust–mantle differentiation and the fate of Niobium. *Earth Planet. Sci. Lett.* **254**, 158–172.

Philpotts J. A. and Schnetzler C. C. (1970) Phenocryst-matrix partition coefficients for K, Rb, Sr and Ba, with applications to anorthosite and basalt genesis. *Geochim. Cosmochim. Acta* **34**, 307–322.

Quartieri S., Antonioli G., Geiger C. A., Artioli G. and Lottici P. P. (1999) XAFS characterization of the structural site of Yb in synthetic pyrope and grossular garnets. *Phys. Chem. Miner.* **26**, 251–256.

Quartieri S., Dalconi M. C., Boscherini F., Oberti R. and D'Acapito F. (2004) Changes in the local coordination of trace rare-earth elements in garnets by high-energy XAFS: new data on dysprosium. *Phys. Chem. Miner.* **31**, 162–167.

Rapp R. P., Shimizu N. and Norman M. D. (2003) Growth of early continental crust by partial melting of eclogite. *Nature* **425**, 605–609.

Ravna E. K. (2000a) Distribution of Fe^{2+} and Mg between coexisting garnet and hornblende in synthetic and natural systems: an empirical calibration of the garnet-hornblende Fe–Mg geothermometer. *Lithos* **53**, 265–277.

Ravna E. K. (2000b) The garnet-clinopyroxene Fe^{2+}–Mg geothermometer: an updated calibration. *J. Metamorph. Geol.* **18**, 211–219.

Righter K. and Shearer C. K. (2003) Magmatic fractionation of Hf and W: constraints on the timing of core formation and differentiation in the Moon and Mars. *Geochim. Cosmochim. Acta* **67**, 2497–2507.

Rubatto D. and Hermann J. (2007) Experimental zircon/melt and zircon/garnet trace element partitioning and implications for the geochronology of crustal rocks. *Chem. Geol.* **241**, 38–61.

Rudnick R. L., Barth M., Horn I. and McDonough W. F. (2000) Rutile-bearing refractory eclogites: missing link between continents and depleted mantle. *Science* **287**, 278–281.

Salters V. J. M. and Hart S. R. (1991) The mantle sources of ocean ridges, islands and arcs – the Hf-isotope connection. *Earth Planet. Sci. Lett.* **104**, 364–380.

Salters V. J. M. and Longhi J. (1999) Trace element partitioning during the initial stages of melting beneath mid-ocean ridges. *Earth Planet. Sci. Lett.* **166**, 15–30.

Salters V. J. M. and Zindler A. (1995) Extreme Hf-176 Hf-177 in the sub-oceanic mantle. *Earth Planet. Sci. Lett.* **129**, 13–30.

Scherer E., Münker C. and Mezger K. (2001) Calibration of the lutetium–hafnium clock. *Science* **293**, 683–687.

Scherstén A., Elliott T., Hawkesworth C. and Norman M. (2004) Tungsten isotope evidence that mantle plumes contain no contribution from the Earth's core. *Nature* **427**, 234–237.

Schmidt A., Weyer S., John T. and Brey G. P. (2009) HFSE systematics of rutile-bearing eclogites: new insights into subduction zone processes and implications for the earth's HFSE budget. *Geochim. Cosmochim. Acta* **73**, 455–468.

Schmidt M. W., Dardon A., Chazot G. and Vannucci R. (2004) The dependence of Nb and Ta rutile-melt partitioning on melt composition and Nb/Ta fractionation during subduction processes. *Earth Planet. Sci. Lett.* **226**, 415–432.

Schnetzler C. C. and Philpotts J. A. (1970) Partition coefficients of rare-earth elements between igneous matrix material and rock-forming mineral phenocrysts – II. *Geochim. Cosmochim. Acta* **34**, 331–340.

Schoenberg R., Kamber B. S., Collerson K. D. and Eugster O. (2002a) New W-isotope evidence for rapid terrestrial accretion and very early core formation. *Geochim. Cosmochim. Acta* **66**, 3151–3160.

Schoenberg R., Kamber B. S., Collerson K. D. and Moorbath S. (2002b) Tungsten isotope evidence from similar to 3.8-Gyr metamorphosed sediments for early meteorite bombardment of the Earth. *Nature* **418**, 403–405.

Schönbächler M., Lee D. C., Rehkämper M., Halliday A. N., Fehr M. A., Hattendorf B. and Günther D. (2003) Zirconium isotope evidence for incomplete admixing of r-process components in the solar nebula. *Earth Planet. Sci. Lett.* **216**, 467–481.

Schönbächler M., Lee D. C., Rehkämper M., Halliday A. N., Hattendorf B. and Günther D. (2005) Nb/Zr fractionation on the Moon and the search for extinct Nb-92. *Geochim. Cosmochim. Acta* **69**, 775–785.

Schönbächler M., Rehkämper M., Halliday A. N., Lee D. C., Bourot-Denise M., Zanda B., Hattendorf B. and Günther D. (2002) Niobium–zirconium chronometry and early solar system development. *Science* **295**, 1705–1708.

Shannon R. D. (1976) Revised effective ionic-radii and systematic studies of interatomic distances in halides and chalcogenides. *Acta Crystallogr. A* **32**, 751–767.

Söderlund U., Patchett J. P., Vervoort J. D. and Isachsen C. E. (2004) The Lu-176 decay constant determined by Lu–Hf and U–Pb isotope systematics of Precambrian mafic intrusions. *Earth Planet. Sci. Lett.* **219**, 311–324.

Tiepolo M., Bottazzi P., Foley S. F., Oberti R., Vannucci R. and Zanetti A. (2001) Fractionation of Nb and Ta from Zr and Hf at mantle depths: the role of titanian pargasite and kaersutite. *J. Petrol.* **42**, 221–232.

Tiepolo M., Vannucci R., Bottazzi P., Oberti R., Zanetti A. and Foley S. F. (2000a) Partitioning of rare earth elements, Y, Th, U and Pb between pargasite, kaersutite, and basanite to trachyte melts: implications for percolated and veined mantle. *Geochem. Geophys. Geosyst.* **1**, 1039.

Tiepolo M., Vannucci R., Oberti R., Foley S., Bottazzi P. and Zanetti A. (2000b) Nb and Ta incorporation and fractionation in titanian pargasite and kaersutite: crystal-chemical constraints and implications for natural systems. *Earth Planet. Sci. Lett.* **176**, 185–201.

Timm C., Hoernle K., Werner R., Hauff F., van den Bogaard P., White J., Mortimer N. and Garbe-Schönberg D. (2010) Temporal and geochemical evolution of the Cenozoic intraplate volcanism of Zealandia. *Earth Sci. Rev.* **98**, 38–64.

Tollstrup D. L. and Gill J. B. (2005) Hafnium systematics of the Mariana arc: evidence for sediment melt and residual phases. *Geology* **33**, 737–740.

Touboul M., Kleine T., Bourdon B., Palme H. and Wieler R. (2007) Late formation and prolonged differentiation of the Moon inferred from W isotopes in lunar metals. *Nature* **450**, 1206–1209.

van Westrenen W., Blundy J. and Wood B. (1999) Crystal-chemical controls on trace element partitioning between garnet and anhydrous silicate melt. *Am. Mineral.* **84**, 838–847.

van Westrenen W., Blundy J. D. and Wood B. J. (2000) Effect of Fe^{2+} on garnet–melt trace element partitioning: experiments in

FCMAS and quantification of crystal-chemical controls in natural systems. *Lithos* **53**, 189–201.

van Westrenen W., Blundy J. D. and Wood B. J. (2001a) High field strength element/rare earth element fractionation during partial melting in the presence of garnet: implications for identification of mantle heterogeneities. *Geochem. Geophys. Geosyst.* **2**, 1039.

van Westrenen W. and Draper D. S. (2007) Quantifying garnet–melt trace element partitioning using lattice-strain theory: new crystal-chemical and thermodynamic constraints. *Contrib. Mineral. Petrol.* **154**, 717–730.

van Westrenen W., Wood B. J. and Blundy J. D. (2001b) A predictive thermodynamic model of garnet–melt trace element partitioning. *Contrib. Mineral. Petrol.* **142**, 219–234.

Vervoort J. D. and Blichert-Toft J. (1999) Evolution of the depleted mantle: Hf isotope evidence from juvenile rocks through time. *Geochim. Cosmochim. Acta* **63**, 533–556.

Vervoort J. D. and Patchett P. J. (1996) Behavior of hafnium and neodymium isotopes in the crust: constraints from Precambrian crustally derived granites. *Geochim. Cosmochim. Acta* **60**, 3717–3733.

Vervoort J. D., Patchett P. J., Albarède F., Blichert-Toft J., Rudnick R. and Downes H. (2000) Hf–Nd isotopic evolution of the lower crust. *Earth Planet. Sci. Lett.* **181**, 115–129.

Vervoort J. D., Plank T., Patchett P. J. and Prytulak J. (2007) Hf and Nd isotopic composition of sediments, old and new. *Geochim. Cosmochim. Acta* **71**, A1065.

Wade J. and Wood B. J. (2001) The Earth's 'missing' niobium may be in the core. *Nature* **409**, 75–78.

Weyer S., Münker C. and Mezger K. (2003) Nb/Ta, Zr/Hf and REE in the depleted mantle: implications for the differentiation history of the crust–mantle system. *Earth Planet. Sci. Lett.* **205**, 309–324.

Weyer S., Münker C., Rehkamper M. and Mezger K. (2002) Determination of ultra-low Nb, Ta. Zr and Hf concentrations and the chondritic Zr/Hf and Nb/Ta ratios by isotope dilution analyses with multiple collector ICP-MS. *Chem. Geol.* **187**, 295–313.

White A. J. R., Chappell B. W. and Jakeš P. (1972) Coexisting clinopyroxene, garnet and amphibole from an eclogite, Kakanui, New-Zealand. *Contrib. Mineral. Petrol.* **34**, 185–191.

White W. M. and Patchett J. (1984) Hf–Nd–Sr isotopes and incompatible element abundances in island arcs – implications for magma origins and crust–mantle evolution. *Earth Planet. Sci. Lett.* **67**, 167–185.

Woodhead J. D., Hergt J. M., Davidson J. P. and Eggins S. M. (2001) Hafnium isotope evidence for 'conservative' element mobility during subduction zone processes. *Earth Planet. Sci. Lett.* **192**, 331–346.

Xiong X. L., Adam J. and Green T. H. (2005) Rutile stability and rutile/melt HFSE partitioning during partial melting of hydrous basalt: implications for TTG genesis. *Chem. Geol.* **218**, 339–359.

Yin Q. Z., Jacobsen S. B., Yamashita K., Blichert-Toft J., Telouk P. and Albarède F. (2002) A short timescale for terrestrial planet formation from Hf–W chronometry of meteorites. *Nature* **418**, 949–952.

Zack T., Foley S. F. and Jenner G. A. (1997) A consistent partition coefficient set for clinopyroxene, amphibole and garnet from laser ablation microprobe analysis of garnet pyroxenites from Kakanui, New Zealand. *N. Jb. Miner. Abh.* **172**, 23–41.

Associate Editor: Frederick A. Frey